Politecnico di Torino

MASTER's Degree in Mechatronic Engineering

A.a. 2025/2026

Sessione di laurea Luglio 2026

Variable Flux Machines for High Performance Drives: Technology Assessment

Relatore:

Paolo Pescetto

Candidati:

Raffaella Zampella

Indice

Elenco delle figure

Capitolo 1

Introduction

The need for more effective and versatile electrical machinery has increased recently due to the global shift toward sustainable energy and transportation. The needs for electric motor technologies are changing as a result of the electrification of mobility, which includes everything from electric and hybrid vehicles (EVs and HEVs) to new uses in industrial drives and renewable energy systems. High-efficiency applications have traditionally relied on conventional permanent magnet (PM) machines. The high torque density, small size, and superior steady-state performance are some of their benefits. Nevertheless, they also have important drawbacks: once the machine is constructed, the air-gap flux is essentially fixed; they perform worse in situations where flux weakening is necessary, and they may experience irreversible demagnetization if exposed to high temperatures or to an excessive current. The development of Variable Flux Machines (VFMs) and, more precisely, Variable Flux Memory Machines (VFMMs) has been accelerated by this technological environment. The efficiency advantages of PM machines are combined with VFMMs' capacity to actively modify and "store" various magnetization states. Practically, this means that the machine can adjust its magnetic flux dynamically to maximize efficiency under low load, boost torque under high demand or minimize losses while cruising. The machine's ability to sustain its magnetization state (MS) without constant excitation is known as its "memory" property, and it is especially useful for cutting down on energy usage. VFMMs have a significant potential impact. For instance, adjusting the magnetic flux to various driving cycles in EVs can directly result in an increased range, a decreased battery usage, and a reduced need for rare-earth magnets. VFMMs have the potential to facilitate flexible and efficient integration with variable-speed generators and turbines in renewable energy systems. These uses demonstrate why, in the past ten years, VFMMs have grown in popularity as a research topic.

1.1 The relevance of VFMMs

Both industry and academia have given VFMMs a great deal of attention since they were first introduced in the early 2010s. By investigating variable-flux PM concepts, control strategies, and thermal effects, researchers have laid the groundwork. A variety of VFMM topologies, such as dual-layer, asymmetric, hybrid magnetic circuit, and leakage-flux designs, have been examined, building upon these foundations. Each topology aims to find a balance between the conflicting demands of maintaining manufacturability, minimizing losses, achieving wide flux regulation, and optimizing torque density. A huge number of academic works on VFMMs were published in the last decade, indicating a robust and expanding interest in the topic. There are two scientific and practical reasons for this increase in research:

- Energy efficiency requirements: more stringent rules relating to emissions and vehicle efficiency encourage the development of technologies that can optimize every watt of energy.

- Material limitations: VFMMs permit a more efficient use of magnetic materials, while reliance on rare-earth magnets opens up problems with the supply chain.

- Design flexibility: VFMMs allow engineers to optimize flux levels across a variety of operating regimes, in contrast to traditional PM machines.

VFMMs have drawbacks despite these benefits. They frequently have more intricate designs requiring for advanced electromagnetic modelling. Without affecting dynamic performance, control algorithms must regulate the magnetization and demagnetization processes. Additionally, the cost and availability of advanced magnetic materials with appropriate coercivity and thermal stability continue to be obstacle to their widespread adoption.
Variable Flux Memory Machines have been developed rapidly in recent years, but the literature available is scattered across a wide variety of machine topologies, material technologies and control strategies. Many studies are available for specific architectures or isolated performance aspects, however it is hard to obtain a unified and structured understanding of the overall design landscape.
Furthermore, direct comparisons among various VFMM configurations are often made under non uniform hypotheses, which prevent the possibility of drawing general conclusions about their relative advantages and disadvantages. Thus, a comprehensive reference framework for designers and researchers to easily determine the trade-offs between performance, complexity, efficiency and material usage is still lacking. n this environment, the need for a systematic and critical overview of VFMM technologies is growing. A systematic analysis of the existing solutions can be useful for identifying design trends, emerging technologies and unresolved issues,

providing useful guidelines for future developments of high-performance electric machines.

1.2 Thesis Objectives

The main goal of this thesis is to present a detailed and organized overview of Variable Flux Memory Machine (VFMM) technologies with particular focus on their configurations, operating principles and electromagnetic performance features. Recent years have seen the rapid development of VFMM architectures, which has resulted in a large body of scientific literature, frequently focusing on specific topologies or individual performance characteristics. However, still few systematic comparisons of the different technological solutions are available, precluding a clear identification of the most suitable design approaches for modern high-efficiency applications.
In this sense, the objective of this thesis is to collect, organize and critically analyze the existing knowledge on VFMM technologies, to highlight the correlations between machine topology, magnetic materials and performance behavior. The work is not only intended to review the existing solutions, but also to highlight the fundamental design trade-offs affecting the efficiency, torque density, flux regulation capability and operational flexibility. The specific objectives of this thesis can be summarized as to satisfy these objectives:

- Discuss and classify the main Variable Flux Memory Machine architectures presented in the literature, including series, parallel, hybrid-magnetic-circuit, switched-flux, and other emerging configurations, describing their structural features and operating principles.

- Analyze the electromagnetic behavior of different VFMM topologies, with particular attention to the most important performance indexes such as torque production, flux regulation capability, back-electromotive force characteristics, efficiency maps, and resistance to accidental demagnetization.

- Compare the studied machine configurations, explaining their advantages and disadvantages and the suitability for different areas of applications.

- Study magnetic materials and the interaction of low and high coercivity permanent magnets. Evaluate the effect of their characteristics on controllability, magnetic stability and general machine performance.

- Identify the main technological barriers currently limiting the widespread adoption of VFMM technologies, including issues related to design complexity, control strategies, thermal effects, material availability, and manufacturing restrictions.

- Provide a structured and coherent reference basis, which integrates the analyzed data to provide a unified perspective, supporting future research activities and making easier the choice of the most suitable design solutions for advanced electrical machine applications.

The general aim of this thesis is to contribute to a better understanding of the Variable Flux Memory Machine technologies, through a systematic and critical synthesis of the existing literature, in order to support the development of more efficient, flexible and reliable electrical machines for the next generation energy and transportation systems.

1.3 Thesis Structure

The thesis is structured as follows to meet the goals listed above:

- The conceptual foundations of VFMMs are covered in Chapter 2, which also examines the underlying magnetic phenomena.
- A comprehensive discussion of the literature is provided in Chapter 3, which is divided into sections on topologies and architectures, control and optimization techniques, construction and material technologies, applications and open research challenges.
- Chapter 4 completes the thesis by summarizing the results and by considering its limitations.

Capitolo 2

Theoretical Foundations

2.1 Overview and Purpose

The theoretical foundation required to fully understand the modelling, performance properties, and operating principles of variable flux memory machines (VFMMs) is provided in this chapter. Permanent magnet (PM) machines' efficiency and torque density are combined with VFMMs' capacity to dynamically control and hold various flux levels. They differ from traditional PM machines due to their "memory" effect, which is made possible by unique magnetic materials. The machine's governing equations, magnetic memory, electromagnetic principles, and modelling techniques which assist in the analysis and optimization of VFMM designs are all covered in the sections that follow.

2.2 Fundamentals of Electromechanical Energy Conversion

The electromechanical energy conversion principle, which uses the interaction of magnetic fields, is the basis for all electric machines.

The electromagnetic torque T_e generated in a rotating machine is expressed as:

$$T_e = \frac{3}{2} p \left(\lambda_d i_q - \lambda_q i_d \right) \tag{2.1}$$

where:

- p = number of pole pairs;
- λ_d, λ_q = flux linkages in the d- and q-axes;
- i_d, i_q = stator current components in the synchronous reference frame.

In conventional PM machines, the flux linkage λ_d depends only on the permanent magnet flux, which is fixed after assembly. VFMMs, instead, allow λ_d to vary by changing the magnetization state (MS) of their permanent magnets.

This capability allows field-weakening for high-speed operations and field-strengthening for high-torque conditions, without the use of separated field windings as in wound-field synchronous machines.

2.3 Concept of Variable Flux and Magnetic Memory

The nonadjustable permanent magnetic field obtained using high coercive force (HCF) rare-earth permanent magnets is one of the limitations of conventional PMSMs. At low speeds, the strong permanent magnetic field generates significant amounts of torque; however, at high speeds, the back-electromotive force (EMF) of PMSMs will surpass the dc source's voltage limit. In order to achieve a wide speed range, a large field weakening current must be used to depress the permanent magnetic field quickly. This leads to additional losses and increases the possibility of unintentional demagnetization. As a result, conventional PMSMs' overall driving cycle efficiency is decreased over a wide speed range. Low coercive force (LCF) magnets are used in variable flux machines (VFMs) as a solution to this problem. The magnetization state (MS) of LCF, often also referred to as VPM (Variable Permanent Magnet), magnets can be changed to control the air-gap flux density by applying a d-axis magnetizing or demagnetizing current. The hysteresis characteristic of LCF magnets allows the MS to be preserved and remembered when the current is cut off. As a result, "memory machines" is another name for this class of machines. Additionally, it takes little time to complete the magnetization and demagnetization processes. VFMs only require a d-axis current pulse, which results in lower losses and higher efficiency than conventional PMSMs, which require a continuous field weakening current at high speed. To simultaneously achieve high torque density and flexible air-gap flux density, hybrid permanent magnet VFMs (HPM-VFMs) that use both LCF and HCF magnets are suggested. Because of their high magnetic energy, HCF magnets, sometimes referred to as CPM (Constant Permanent Magnet), help to generate more torque, while LCF magnets continue to be used because their MS is controllable. VFMMs work best with permanent magnets (PMs) that have a linear demagnetization curve, a knee point in the second quadrant, and a moderate to low level of H_c and high remanence (B_r). AlNiCo, ferrite, and SmCo magnets are employed as low-H_c magnets in VFMMs in the existing literature. Fig. 2.1 shows the demagnetization curves for three types of common low-Hc magnets. Considering using only the AlNiCo magnet, the torque density of VFMM obtained using a single low-H_c is relatively limited because of the low magnetic energy product of the AlNiCo magnet. The hybrid-magnet VFMMs, which can be divided into series-magnet configuration and parallel-magnet configuration, developed quickly to increase the torque density by using a type of low-H_c magnet and NdFeB magnet (high coercive force magnet).

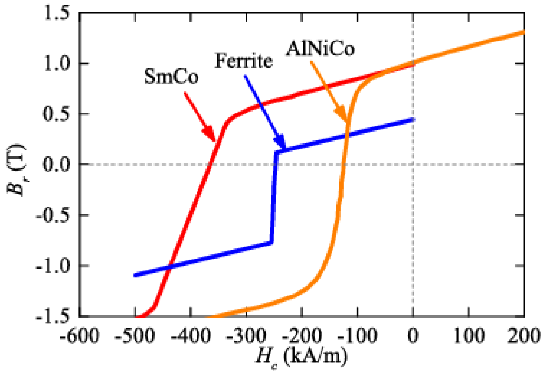

Figura 2.1: Demagnetization curves of typical Low-Hc magnets.
Source: [17]

Capitolo 3

Existing Technologies

3.1 Classification of VFMM Topologies

In their 2015 U.S. patent US20150340915A1, which was co-developed by Nissan Motor Co. and the Wisconsin Electric Machines and Power Electronics Consortium (WEMPEC), Kato, Lorenz, and Limsuwan detailed one of the first applications of a controllable magnetic flux path in permanent magnet (PM) machines. The invention presented the idea of a variable magnetic flux-type rotary machine, where the magnetic flux generated by the PMs is controlled by armature reaction and magnetic circuit design without changing the magnetization of the magnets. The rotor has magnetic field-impeding components and flux bypass paths that regulate the air-gap flux in accordance with the operating current. With an optimized condition $\frac{\partial K_T(I)}{\partial I} \approx 0$ in the non-saturated range, this configuration guarantees that the torque constant K_T varies as a function of the stator current I, according to the relationship $T_r = K_T(\mathrm{I}) \times \mathrm{I}$. Without the need for magnetization or demagnetization control, this produces a wide variable-speed range, high torque at high loads, and low loss at light loads. Rotors with one to three permanent magnets per pole, varying angular orientations (radial, tangential, and hybrid), and combinations of magnetic flux bypass gaps and impeding bridges were among the various embodiments and design variations that were suggested. The objectives of these structures were to increase torque production, reduce magnetic leakage, and boost efficiency over a large operating range. Later designs of the Variable Flux Memory Machine (VFMM) and Hybrid Magnetic Circuit (HMC), which advanced the idea of magnetic flux control using low-coercivity magnets and circuits assisted by magnetization, were made possible by this invention. This innovative method can be considered the direct ancestor of modern VFMMs, such as Switched-Flux and Hybrid-Series/Parallel topologies. In general, hybrid magnet VFMMs fall into one of two categories: series or parallel. The design trade-offs in the current

VFMMs with either series or parallel magnetic circuit structures constitute the main difficult problem. The series VFMM has a relatively restricted flux regulation range, whereas the parallel-type VFMM's LCF PMs typically show a significant on-load demagnetization effect. Consequently, an alternative hybrid-magnetic-circuit VFMM (HMC-VFMM) type is considered. The suggested HMC-VFMM offers the unique benefit of useful unintentional demagnetization (UD) withstand capability in series type and good flux regulation capability in parallel type.

Topologies
Series Hybrid VFMM
Parallel Hybrid VFMM
Hybrid Magnetic Circuit VFMM (HMC-VFMM)
Hybrid-PM Switched Flux Memory Machine (SFMM)
External-Rotor Switched Flux Memory Machine
Fault-Tolerant Flux Switching Memory Machine
Variable Magnetization Pattern Machine (VMPM)
Variable-Magnetization IPM (VM-IPM)
Axial-Field Juxtaposed Magnetic Circuit VFMM
Dual-Sided VFMM
Variable Leakage Flux IPM Machine
Iron-Nitride-Based PM VFMM
Hybrid-Excited Flux-Modulated Memory Machine

Tabella 3.1: Classification of VFMM examined topologies

3.2 VFMM with Series Hybrid Magnets

3.2.1 Operating principle

To analyze the machine with series structure is taken into consideration a machine (shown in Fig. 3.1) which uses a three-phase 48-stator-slot/8-rotor-pole structure comparable to the commercial Toyota Prius2010 IPM machine. V-shaped PMs are used to increase the available PM flux, and the full-pitched armature winding and IPM rotor are adopted to obtain the reluctance torque. Additionally, HCF PMs and LCF PMs are are alternatively located on distinct rotor poles, that is, one rotor pole has HCF magnets and the one next to it has LCF magnets. While all LCF magnets have a different polarity, all CPMs are magnetized with the same polarity. The HCF and LCF PMs are therefore magnetically connected in series. Variable magnetization is a feature of VFM machines that depends on VPM characteristics. Figure 3.2 illustrates how the VPM works in an open circuit. The nonlinear B-H curve (B: Flux density, H: Magnetic field strength) in Quadrant II makes it simple to alter the VPM's magnetization state with an external field. For example, if a large demagnetization magnetomotive force (MMF) is applied, the initial working point A will move to point B, which is lower than the knee point. When the negative MMF is released, the working point will then travel along the recoil line BD and come to an end at point C. The working point may then move to point F along the CDEF curve if a magnetization MMF pulse is applied, indicating that magnetization has been applied.

As a result, it is discovered that applying various MMF pulses allows for flexible variation of the VPM working point. Fig. 3.3 simplifies the magnetic circuit of a series connection, with FCPM, FVPM, Rm CPM, and Rm VPM standing for the corresponding MMFs and intrinsic reluctance of CPM and VPM, respectively, while the equivalent external d-axis reluctance is denoted by Rmd. It is visible that since the CPM flux must pass through the VPM, it naturally helps the VPM to resist the accidental demagnetization created by the armature reaction. When the CPMs are present in a series hybrid PM connection, the VPM working points, as shown in Fig. 3.2, would move from points A, C, and F to points A', C', and F', respectively. As a result, the CPM increases and stabilizes the flux density in the VPM. On the other hand, the CPM flux may short-circuit via the VPM branch

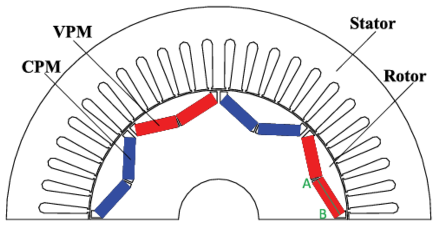

Figura 3.1: Cross section of the studied series Hybrid VFMM.
Source: [8]

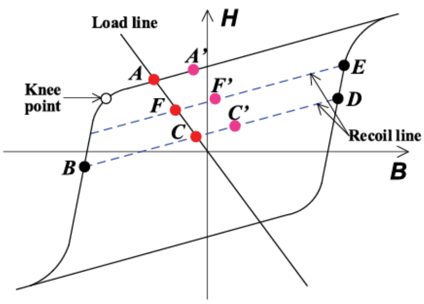

Figura 3.2: VPM working point.
Source: [8]

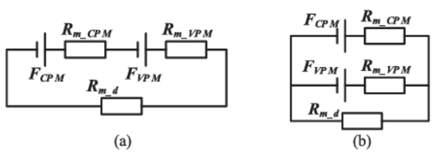

Figura 3.3: series and parallel connections between VPM and CPM.
Source: [7]

in the conventional parallel connection depicted in Fig. 3.3, and it is unable to assist VPM in withstanding the unintentional demagnetization. If two branches are not balanced, the CPM even demagnetizes the VPM. The VPM may be readily demagnetized in parallel hybrid PM VFM machines, as evidenced by the fact that the working point of the VPM with a parallel hybrid PM connection would be lower than that one without a CPM. The complex flux barriers employed to reduce cross-coupling and stop demagnetization in conventional VFM machines can be avoided because series hybrid PM VFM machines naturally have an enhanced capacity to withstand inadvertent demagnetization. This increases the mechanical strength and makes the machine design much simpler. More significantly, during torque generation, -i_d current becomes acceptable, which facilitates the obtaining of the reluctance torque.

3.2.2 Electromagnetic performance and Efficiency

The electromagnetic performance of the suggested VFM machine has been carefully evaluated using 2-D FE analysis, and two typical states, that is, fully forward or fully reverse magnetized VPMs, are presented. Fig 3.5 shows the list of the machine's primary design parameters; the armature and stator windings are identical to those of the Prius2010 IPM machine. The materials SmCo and NdFeB PM are utilized as VPM and CPM, respectively. Figure 3.2.2.1 illustrates the open-circuit field distributions in the two magnetization states. In the fully forward magnetization state, all PMs are inwardly magnetized, whereas in the fully reverse state, the VPMs are outwardly magnetized and the CPMs are inwardly magnetized.

As seen in Fig. 3.4 (a) and (c), the flux is clearly easy to pass through the VPMs, and higher flux densities are visible in the forward magnetization state. Conversely, the flux densities that result from the fully reverse magnetization state are much lower than those of the previous state, even though the CPMs are powerful enough to oppose the VPMs and cause the flux to flow outward in the VPMs. The magnetic saturation in the rotor iron bridges is severe because the flux lines prefer to avoid the VPMs. Furthermore, Figure 3.6 compares the open-circuit radial flux densities on air gap; the waveforms in the fully forward state are totally higher than those in the fully reverse state, indicating a significantly higher fundamental value. A large range of flux variation is implied by the notable difference in amplitudes between the air-gap flux densities in the two states. In the meantime, even when the VPMs are reversely magnetized, the rotor pole-pair number remains constant because the flux density periods are maintained constant in both states.

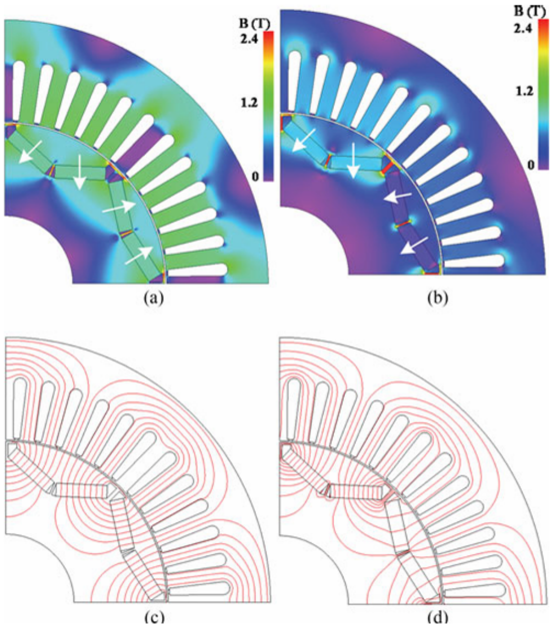

b

Figura 3.4: Open-circuit field distributions in fully forward and reverse magnetization states. (a) Flux density, forward magnetization. (b) Flux density, reverse magnetization. (c) Flux line, forward magnetization. (d) Flux line, reverse mag netization.
Source: [7]

Parameter	Value
Phase number	3
Slot number	48
Pole number	8
Axial length	50.8 mm
Stator outer diameter	264 mm
Stator inner diameter	161.9 mm
Rotor outer diameter	160.44 mm
Rotor inner diameter	68 mm
Air-gap length	0.73 mm
Steel grade	35H270
Number of turns per coil	11
Number of coils per phase	8
CPM B_r	1.2 T
CPM H_c	915 kA/m
CPM thickness	6.5 mm
VPM B_r	1.14 T
VPM H_c	335 kA/m
VPM thickness	7 mm
Rated current density	26.8 A/mm^2

Figura 3.5: Key design parameter of considered VFM machine.
Source: [7]

Figure 3.7 shows the phase back-electromotive forces (back-EMFs) in the two states at 1500 r/min. The forward and reverse states' corresponding fundamental amplitudes are 117 V and 48 V, respectively, indicating that a maximum available flux variation range of 41% to 100% can be achieved. The cogging torques in the fully forward and reverse magnetization states are displayed. As the rotor pole-pair number remains constant across states, the cogging torque cycle numbers are the same (Fig. 3.8). However, because of the stronger magnetic field, the cogging torque amplitude in the forward state is noticeably larger. One of the main advantages of the suggested

VFM machine over the traditional VFM machines is its high torque density, which will be thoroughly examined.

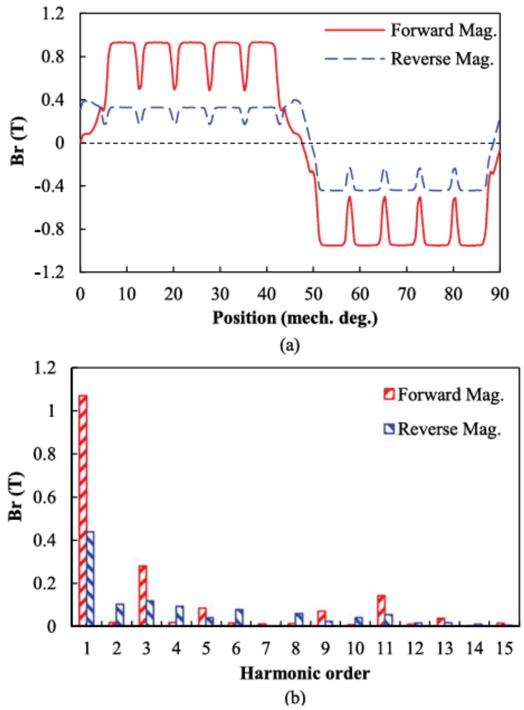

Figura 3.6: Open-circuit air-gap radial flux densities in fully forward and reverse magnetization states. (a) Waveforms. (b) Spectra.
Source: [7]

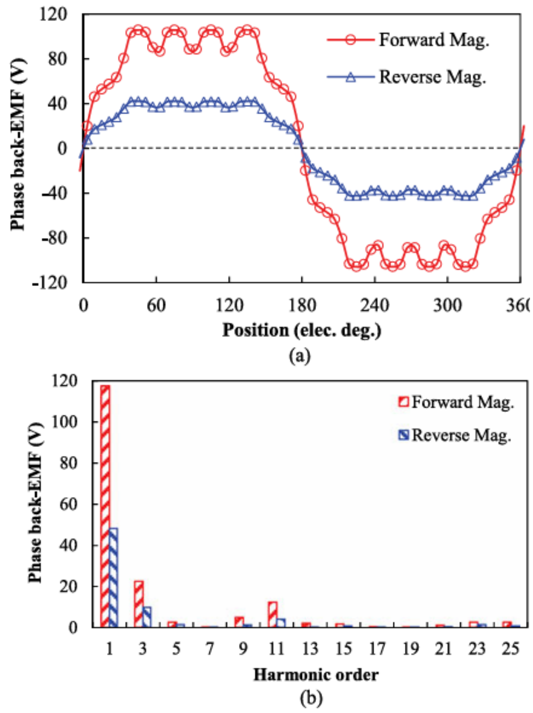

Figura 3.7: Open-circuit phase back-EMFs at 1500 r/min in fully forward and reverse magnetization states. (a) Waveforms. (b) Spectra.
Source: [8]

With rated current amplitudes of 236 A, Fig. 3.9 shows the average torque versus current angle, or the phase angle between phase current and open-circuit back-EMF. In the forward magnetization state, it can be seen that the peak torque roughly occurs at 40°, and a considerable reluctance torque (roughly 25% of the total torque output) is obtained. These CPMs and VPMs' magnetic connections significantly increase their resistance to unintentional demagnetization. The reluctance torque has been restored since applying $-i_d$ is safe. As a result, the suggested VFM machine inherits the reluctance torque, a feature of IPM machines that improves the overall torque density. Although the reluctance torque is still present, the torque output is much reduced in the reverse magnetization state because of the weaker magnetic field. Figure 3.10 illustrates the corresponding torque waveforms at the current angle of 0° and the current angle with the highest torque, respectively.

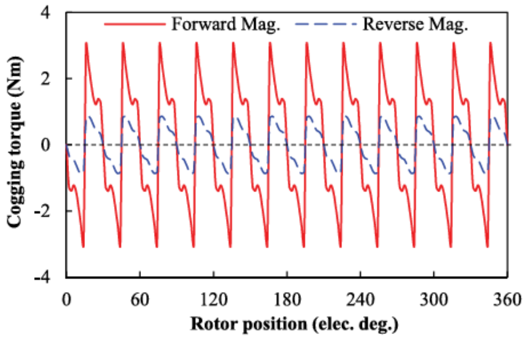

Figura 3.8: Cogging torques in fully forward and reverse magnetization states.
Source: [8]

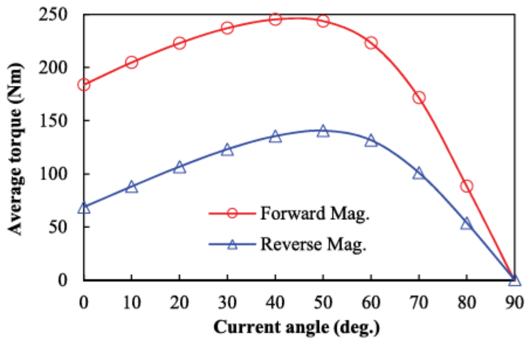

Figura 3.9: Average torque versus current angle in fully forward and reverse magnetization states.
Source: [7]

Additionally, Fig. 3.11 shows the average torque versus i_q in the fully forward magnetization state, although the highest torque is shown at each point by the average torque versus current amplitude under the current angle. It is evident that as current amplitudes increase, so does the ratio of the reluctance torque to the total torque. The unintentional demagnetization brought on by i_q should not affect

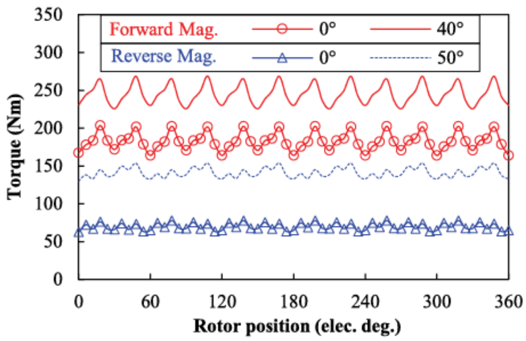

Figura 3.10: Torque waveforms in fully forward and reverse magnetization states.
Source: [7]

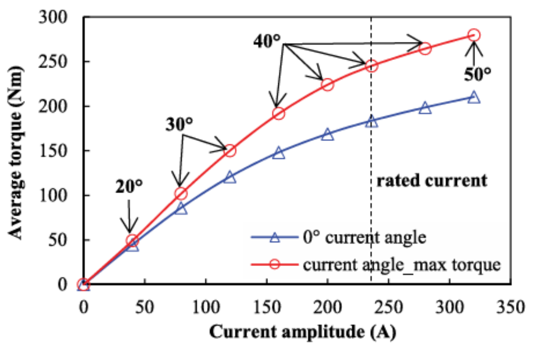

Figura 3.11: Average torque versus current amplitude with different current angle in the fully forward magnetization states.
Source: [7]

the VFM machines. The analysed series hybrid PM VFM machine can maintain the VPM's working point independent of i_q with the help of CPMs. The fundamental back-EMFs at 1500 r/min resulting from different excitations, based on the fully forward magnetization state, are shown in Fig. 3.12. Even at very high currents, the back-EMFs only slightly decrease. The re-magnetization from the fully reverse magnetization and the demagnetization from the fully forward magnetization are shown in Fig. 3.13, where the fundamental back-EMFs corresponding to $+i_d$ (re-magnetization) and $-i_d$ (demagnetization) are present. When roughly three times the rated current is applied, the VPMs can be completely demagnetized to the opposite polarity depending on the fully forward magnetization state. The complete

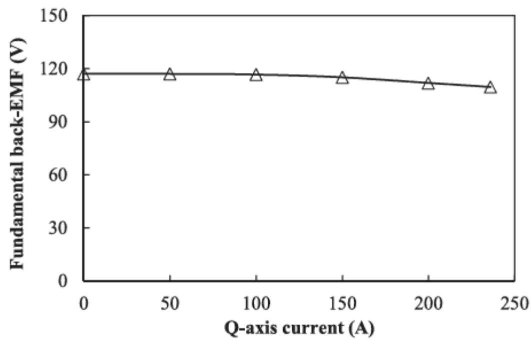

Figura 3.12: Peak fundamental phase back-EMFs at 1500 r/min after different i_q excitations from fully forward magnetization state.
Source: [7]

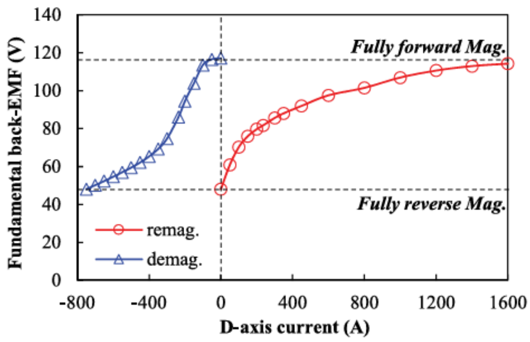

Figura 3.13: Peak fundamental phase back-EMFs at 1500 r/min after different positive and negative id excitations.
Source: [7]

re-magnetization can then be achieved by injecting approximately six times the rated current. The working points of the VPM are specified in Fig. 3.14, which also examines and presents the magnetization characteristics of the VPM during demagnetization and magnetization. The open-circuit working point of the VPM is initially located at point M, one of the stable regions on the demagnetization curve, in the fully forward magnetization state. The irreversible demagnetization would then occur when the working point moved below the knee point with i_d = -150A. Additionally, as i_d increases, the working points in Quadrants II and III continuously decrease along the demagnetization curve, and applying i_d = -2000 A would completely demagnetize the VPM.

It should be mentioned that this current is significantly greater than the previously demonstrated current needed for complete demagnetization, which will be discussed below. Point N in the fully reversed magnetization state is where the VPM working point is located. The VPM has already been partially re-magnetized by the CPM in open-circuit conditions, considering that the magnetization polarities of the VPM and CPM are intrinsically opposite when the VPM is in the state of reverse magnetization. The VPM working points continuously increase as +id increases. $+i_d$ = 1600A yields the complete magnetization. The working point would return to point M following the release of the current once the VPM had fully re-magnetized. As a result, the VPM working point can be conveniently changed by applying various ids, which allows for a variety of PM flux. The CPM in the considered VFM machine supports the re-magnetization of the VPM, although it is still difficult because the magnetic saturation is severe during magnetization. However, even when -i_d is used for the purpose of demagnetization, the VPM is hard to be demagnetized with the help of the CPM. However, since the VPM would shift to point N automatically as a result of the re-magnetization of CPM, it is actually not required to demagnetize it to the lowest working point by i_d = -2000 A. Demagnetizing the VPM to the working point P is therefore sufficient, and once the current is released, it will proceed automatically to point N following the recoil line PN. Consequently, complete demagnetization has also been achieved while the necessary current is noticeably lower.

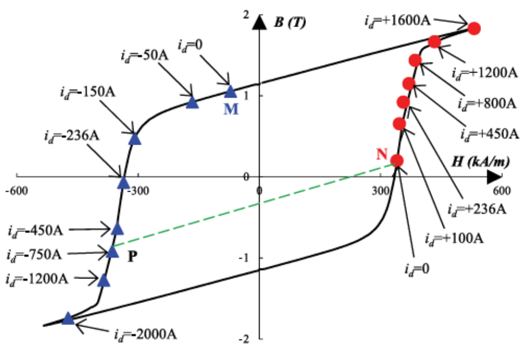

Figura 3.14: Working points of the VPM during demagnetization and magnetization.
Source: [7]

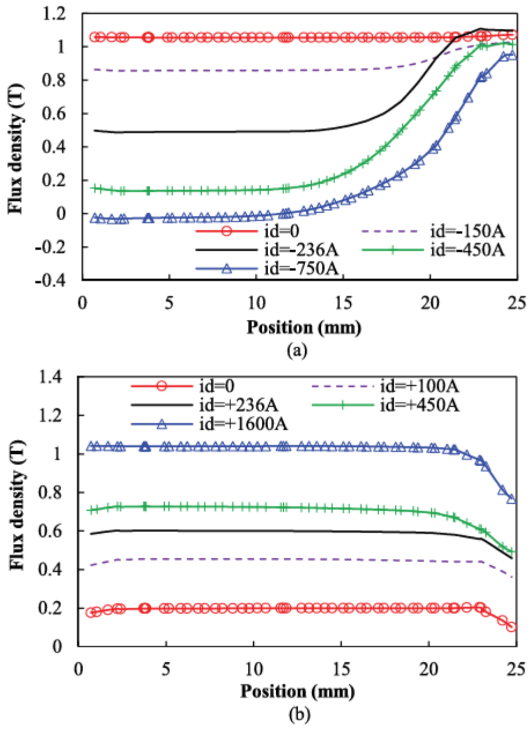

Figura 3.15: Flux densities in the central line inside the VPM after demagnetization and re-magnetization. (a) Demagnetization from fully forward magnetization state. (b) Re-magnetization from fully reverse Magnetization state.
Source: [8]

A monitoring line AB inside the VPM is used to further illustrate the magnetic properties in the demagnetization and remagnetization. It should be mentioned that when i_d is applied, the two VPM pieces in a single rotor pole are symmetrical. Following demagnetization and remagnetization, the flux densities along the magnetization direction on the monitoring line AB are shown in Figs. 3.15(a) and (b), respectively. Based on the fully forward state, i_d = -750 A can roughly demagnetize the VPMs, and i_d = 1600 A can return the VPMs to the fully forward state. However, it should be highlighted that while the VPM portions near the d-axis position are easily demagnetized or re-magnetized by i_d, the portions near the q-axis position are more challenging to modify. Therefore, if the VPMs are not completely demagnetized or re-magnetized, there may be uneven field distributions inside of them. This could lead to an increase in spatial harmonics and local saturation, which could negatively impact the machine performance. The VPMs can be magnetized or demagnetized with the correct id, according to the earlier analysis, and if i_d is high enough, the full magnetization and demagnetization states are obtained. Since severe saturation happens when a high i_d is applied, the magnetic saturation has a major impact on the necessary demagnetizing and magnetizing currents. It should be noticed that the full flux variation range is not always required; instead, a comparatively smaller variation range may be used, which would lower the necessary demagnetizing and magnetizing currents. VPMs can be demagnetized to reveal the fundamental back-EMF of about 63 V, as illustrated in Fig. 3.13, with the study system's 450 A current limit. This is 54% higher than the back-EMF in the full forward magnetization state (54% magnetization state). The elimination of the continuous -i_d during high-speed operation, which results in increased efficiency, is a significant advantage of VFM machines. The efficiency map of the considered VFM machine is predicted using a bus voltage of 650 V and a current limit of 236 A. The FE method is used to sweep the copper and iron losses with varying currents, resulting in the best efficiency at every operation point. The efficiency maps in the fully forward and the 54% magnetization states are shown in Fig. 3.16(a) and (b), respectively. It is observable that the fully forward magnetization state produces the higher torque output, and the low speed high-torque region has the highest efficiency. On the other hand, the efficiency in the high speed low torque region is considerably improved, even though the torque output is sacrificed in the 54% magnetization state. As a result, it is advantageous to flexibly switch the magnetization state at various operation regions, such as full magnetization, while partial magnetization occurs in the high-speed region and high-torque region. Consequently, an efficiency map that combines the benefits can be built as illustrated in Fig. 3.16(c). For the manufactured prototype machine the stator of the Prius2010 IPM machine has been directly employed, but the rotor is different. The non-magnetized SmCo PMs are used, indicating that subsequent magnetization is necessary for SmCo PMs, whereas the NdFeB PMs have been

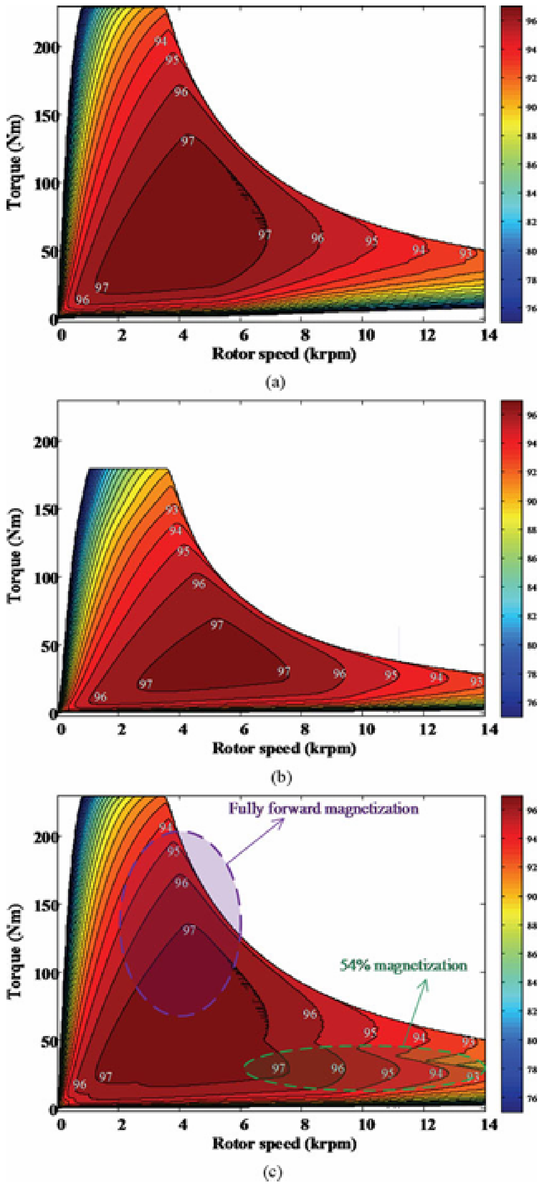

Figura 3.16: Efficiency maps in different magnetization states. (a) In the fully forward magnetization state. (b) In the 54% magnetization state. (c) Integration of the two magnetization states.
Source: [7]

fully magnetized before inserting into the rotor.

3.2.3 Benefits and Drawbacks

The following conclusions can therefore be drawn:

- The series-connected hybrid magnet design improves torque density, flux controllability, and overall efficiency.
- Magnetizing/demagnetizing currents are high, but they can be reduced by optimizing the geometry and materials.
- it's an adequate design for electric vehicle applications, thanks to high performance and operational flexibility.

3.3 Comparative Analysis: Parallel or Series Hybrid Magnets

3.3.1 Configuration and operating principle

For the purpose of boost the torque density of VFM machines, hybrid permanent magnet configurations have been recommended, in which the VPMs supply an extra variable component while the CPMs supply a constant field. The benefits of both the high torque density of traditional PM machines and the good flux controllability of VFM machines can be combined by magnetically connecting the two types of magnets in series or parallel. Since the CPMs and VPMs are mounted on the same rotor pole, the CPMs' flux tends to avoid the VPMs. Therefore, the total effective flux is the sum of that created by the CPMs and VPMs, that is, a parallel connection between the two types of magnets. Nevertheless, in this configuration, the VPM's operating point is unstable and susceptible to automatic demagnetization by the adjacent CPM. Rather, VFM machines that have series connections between the CPM and the VPM, which allows the CPM's flux to flow through the VPM and stabilize its operating point. It is possible to mount the CPM and VPM in series on the same pole. Another option is to mount the VPM and CPM alternately on two adjacent rotor poles, with all of the VPMs having the same polarity and all the CPMs having the opposite polarity. Two VFM machines using parallel and series hybrid PMs are compared to determine their differences based on the commercial Toyota Prius 2010 IPM machine dimensions and the common flux-weakening salient IPM topology. This comparison may provide guidelines for the design and analysis of VFM traction machines. Fig. 3.17(a) and (b) display the cross sections of the parallel and series hybrid VFM machines, respectively. The two machines have identical overall dimensions. The V-shaped IPM rotor

topology is also used, and the 48-stator-slot/8-rotor-pole structure and distributed armature windings are identical to those of the Prius 2010 IPM machine. For CPM and VPM, respectively, NdFeB and SmCo materials are utilized. The torque and flux-regulation performance of the two machines is compromised by optimizing the PM thickness and flux barriers. Two CPMs are positioned on each rotor pole and next to the d-axis position in the parallel hybrid VFM machine shown in Fig. 3.17(a); two additional VPMs are positioned at the side of the CPMs and near the q-axis position. To reduce cross coupling and support the maintenance of the VPMs' operating point, numerous flux barriers are placed on the rotor. Actually, in order to prevent accidental demagnetization, these flux barriers are typically required in single VPM or parallel hybrid VFM machines. The series hybrid VFM machine, on the other hand, has a rather straightforward configuration, that can be seen in Fig. 3.17(b), which is comparable to the standard IPM machine but alternately places CPMs and VPMs on every two adjacent poles. In this way, every VPM has the same polarity, whereas every CPM has the opposite. Because of the help of CPMs, the VPM working point is naturally stable, avoiding the complex rotor flux barriers. The magnetization polarities of PMs are indicated by the arrows in Figure 3.17, and the two VFM machines allow for the adjustment of VPM polarities (referring to Figure 3.17(a) and (c) for the parallel hybrid machine and Figure 3.17(b) and (d) for the series hybrid machine). As can be observed, the VPM has a knee point, that is the point at which the demagnetization curve becomes nonlinear, which is high in Quadrant II and it has a relatively low coercive force (H_c). As a result, the VPM's magnetization state is easily changed. For example, if the VPM working point is pushed from the starting point A to point B, which is below the knee point, due to a high negative magnetomotive force (MMF), it will recover along the recoil line BD and conclude at point C once the MMF is released. As a result, the planned demagnetization has been achieved, and the new remanent flux density (B_{rk}) is less than the old one (B_r). The resulting state of the VPM can be shown as follows by introducing a magnetization ratio factor k_m:
$k_m = \frac{B_{rk}}{B_r}$
The VPM working point may then move to point F along the curve CDEF, which represents another remanent flux density, if a high positive MMF is applied and then released. The variable flux in the VFM machine is the result of the flexible regulation of the VPM MS. In contrast, it is challenging to alter the remanent flux density in Quadrant II due to the linear demagnetization curve of CPM, and it can be seen in Fig. 3.18(b). Because of the functions of CPMs, the hybrid PM VFM machines would have a slightly different VPM working point. The CPM flux may short-circuit through the VPM and work against the VPM because the VPMs and CPMs are positioned in parallel in the parallel hybrid machines. Consequently, as shown in Fig. 3.18(a), the open-circuit working points of VPM would be forced downward, that is, from points A, C, and F to points A_p, C_p, and F_p, respectively.

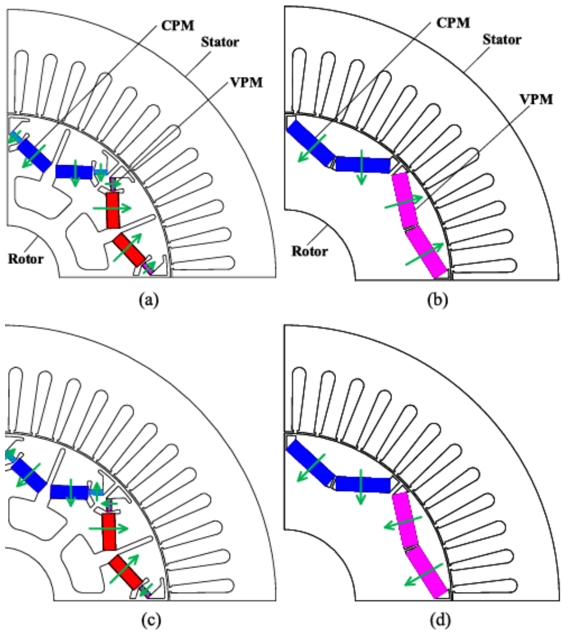

Figura 3.17: Cross sections of parallel and series hybrid VFM machines. (a)Parallel hybrid with forward magnetized VPM. (b) Series hybrid with forward magnetized VPM. (c) Parallel hybrid with reverse magnetized VPM. (d) Series hybrid with reverse magnetized VPM.
Source: [8]

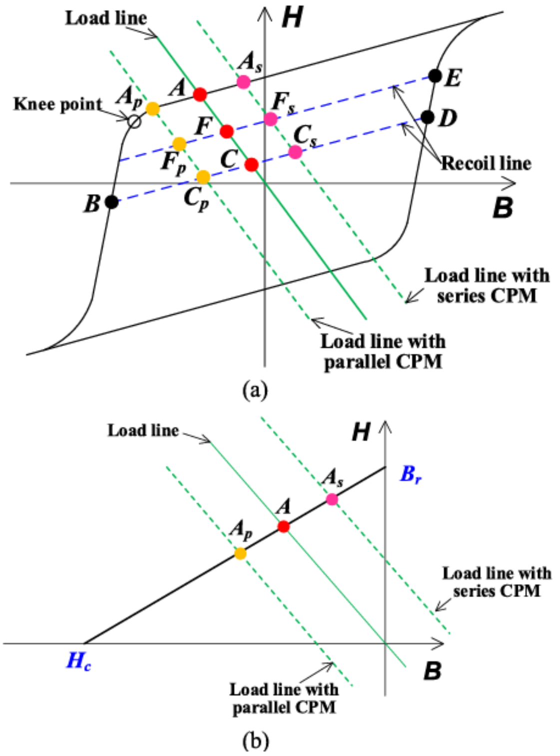

Figura 3.18: Illustration of working point of PM in open-circuit condition (B: flux density, H: magnetic field strength). (a) VPM. (b) CPM.
Source: [8]

As a result, the parallel hybrid connection would have lower VPM working points than those without CPM, suggesting simpler demagnetization. In contrast, the CPM flux would move through the VPM in series hybrid machines, helping it to stabilize the working point. As a result, the VPM working points are pushed positively to A_s, C_s, and F_s, respectively; that is, the CPM increases the flux density in the VPM, and the work points stabilize.

3.3.2 Equivalent Magnetic Circuits

The corresponding magnetic circuits for the parallel and serial hybrid PMs are shown in Fig. 3.19(a) and (b), respectively, to better depict their characteristics. R_g is the equivalent air-gap reluctance, while F_1 (F_2) and R_{m1} (R_{m2}) stand for

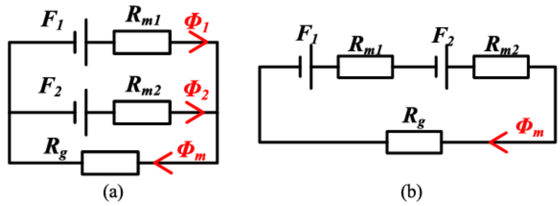

Figura 3.19: Illustration of parallel and series flux paths. (a) Parallel. (b) Series. Source: [8]

the intrinsic MMF and the reluctance of CPM (VPM). The main flux through the air-gap (Φ_{mp}) in the parallel circuit is equal to the sum of the two parallel branches, or the VPM flux (Φ_2) and CPM flux (Φ_1). The following is an expression for the corresponding flux based on the fundamental principle:

$$\Phi_{mp} = \Phi_1 + \Phi_2 \tag{3.1}$$

$$\Phi_1 = \frac{R_{m1}}{R_{m1} + \dfrac{R_{m2}R_g}{R_{m2}+R_g}} F_1 - \frac{\dfrac{R_{m1}R_g}{R_{m1}+R_g}}{\dfrac{R_{m1}R_g}{R_{m1}+R_g} + R_{m2}} F_2 \tag{3.2}$$

$$\Phi_2 = \frac{R_{m2}}{R_{m2} + \dfrac{R_{m1}R_g}{R_{m1}+R_g}} F_2 - \frac{\dfrac{R_{m2}R_g}{R_{m2}+R_g}}{\dfrac{R_{m2}R_g}{R_{m2}+R_g} + R_{m1}} F_1 \tag{3.3}$$

It should be mentioned that if the VPM MMF(F_2) is excessively low, the CPM flux may flow against the VPM and the VPM flux (Φ_2) may be negative. As a result, if the two branches are not balanced, the CPM flux may short circuit via the VPM branch and even demagnetize the VPM. Consequently, in the parallel hybrid configuration, the cross coupling between the VPM and the CPM is severe, that leads to the VPM's working point to become unstable. Furthermore, the PM dimensions and properties can be used to express the intrinsic MMF and reluctance of PM as follows:

$$R_{m1} = \frac{t_1}{\mu_{r1}\,\mu_0\,A_1} \tag{3.4}$$

$$R_{m2} = \frac{t_2}{\mu_{r2}\,\mu_0\,A_2} \tag{3.5}$$

$$F_1 = H_{c1}\,t_1 = \frac{B_{r1}\,t_1}{\mu_{r1}\,\mu_0} \tag{3.6}$$

$$F_2 = H_{c2}\,t_2 = \frac{k_m\,B_{r2}\,t_2}{\mu_{r2}\,\mu_0} \tag{3.7}$$

where μ_0 is the magnetic permeability of air, and t_1 (t_2), A_1 (A_2), B_{r1} (B_{r2}), H_{c1} (H_{c2}), and μ_{r1} (μ_{r2}) are the thickness, cross-section area perpendicular to the magnetization direction, remanent flux density, coercive force, and relative permeability of CPM (VPM), respectively. The primary flux through the air gap in the parallel hybrid PMs is obtained:

$$\Phi_{mp} = \frac{B_{r1}A_1 + k_m B_{r2} A_2}{1 + R_g \mu_0 t_1 t_2 A_1 A_2 \left(A_1 t_2 \mu_{r1} + A_2 t_1 \mu_{r2}\right)/(t_1 + t_2)} \tag{3.8}$$

In contrast, the series hybrid circuit has a single magnetic path, and the CPM flux always passes through the VPM. As a result, the CPM naturally helps the VPM resist unintentional demagnetization. The primary flux that passes through the two types of PMs is represented as follows:

$$\Phi_{ms} = \frac{F_1 + F_2}{R_{m1} + R_{m2} + R_g} \tag{3.9}$$

When (3.4)–(3.7) are substituted into (3.9), the result is:

$$\Phi_{ms} = \frac{A_1 A_2 \left(\mu_{r2} B_{r1} t_1 + k_m \mu_{r1} B_{r2} t_2\right)}{\mu_{r2} A_2 t_1 + \mu_{r1} A_1 t_2 + R_g \mu_0 \mu_{r1} \mu_{r2} A_1 A_2} \tag{3.10}$$

It is evident from (3.8) and (3.10) that, by altering the VPM magnetization state, or modifying the value of k_m, the resulting PM flux in the parallel–series hybrid VFM machines can be controlled. Furthermore, it is observed that the VPM's operating point in the series hybrid configuration is more stable than its parallel counterpart.

3.3.3 Comparative Analysis of Electromagnetic Performance

This section addresses the comparison of the electromagnetic performances of the parallel and series hybrid VFM machines, carried out through the 2-D FE method. In the two standardized magnetization states, VPM fully forward magnetized (K_m=1) in Fig. 3.20 (a) and (c) and VPM fully reverse magnetized (K_m=-1) in Fig. 3.20(b) and (d), Fig. 3.20 illustrates their open-circuit field distributions. Together with the forward magnetized VPM, the CPM contributes to an airgap field in the parallel hybrid machine, as shown in Fig. 3.20 (a). Alternative, when the VPM is reverse magnetized, the CPM flux short-circuits through it and the resulting air-gap field decreases significantly (see Fig. 3.20 (b)). With the VPM forward magnetized, the CPM flux readily passes through the VPM and produces a powerful air-gap field in the series hybrid machine, as can be seen in Fig. 3.20 (c). The alternating CPM and VPM poles in this series hybrid machine, however, have the same polarity when the VPM is reverse magnetized. The rotor field's polarity is still guaranteed by the strong CPM, but the CPM flux finds it much harder to pass through the VPM, resulting in a clearly weaker field, that can be seen in Fig. 3.20 (d). The two

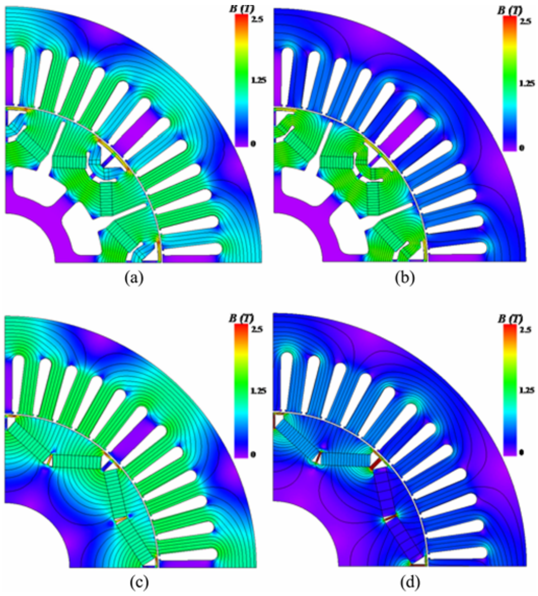

Figura 3.20: Open-circuit field distributions in the two typical magnetization states. (a) Parallel hybrid with forward magnetized VPM (K_m=1). (b)Parallel hybrid with reverse magnetized VPM (K_m=-1). (c) Series hybrid with forward magnetized VPM (K_m=1). (d) Series hybrid with reverse magnetized VPM (K_m=-1).
Source: [8]

machines' notable variations in the forward and reverse magnetization states suggest that the flux variation ranges are huge. Both forward state's flux density amplitudes are noticeably greater than the reverse state's. It is discovered that in both forward and reverse states, the two machines consistently lack even-order harmonics. In fact, the winding configuration that produces the symmetrical phase back-EMFs free from the even order items cancels out the even order spatial harmonics in the series hybrid VFM machine. Furthermore, both machines exhibit considerable back-EMF variation ranges, with the parallel hybrid machine exhibiting ranges of 45% to 100% and the series counterpart exhibiting ranges of 41% to 100%. The parallel and series hybrid VFM machines' torque capacities are examined. Because of the high back-EMFs, the forward magnetization state can produce the most torque. It goes without saying that the reluctance torque is minimal in a parallel hybrid machine but substantial in a series one. This can be explained by the fact that the advanced rotor flux barriers in the parallel hybrid VFM machine sacrifice the rotor saliency ratio, while the $-i_d$ component would significantly demagnetize the VPMs and weaken the PM field. On the other hand, the series hybrid VFM machine removes the complex flux barriers and the $-i_d$ component is acceptable during torque generation, which is how the reluctance torque is obtained, because of its improved ability to withstand unintentional demagnetization. As a result, the series hybrid machine's peak torque is substantially greater than its parallel equivalent. Since the slot/pole combinations in the two machines are the same, the cycle number of torque ripples during a single electric period is always 12. The series hybrid VFM machine consistently shows greater torque than the parallel one when the current angle is fixed at 0°. Furthermore, the benefit of the series hybrid machine can be further increased by fixing the current angle at 45° to incorporate the reluctance torque. In VFM machines, demagnetization caused by q-axis current (i_q) is unfavourable and could inadvertently affect machine performance. First, a monitoring line that is positioned at the centre of VPM and perpendicular to the magnetization direction is used to analyse the effects of CPM on the VPM in the two hybrid configurations. It is evident that the series-connected CPM gives the VPM the forward flux and helps it magnetize, whereas the VPM parallel to the CPM supplies the reversed flux and tends to be demagnetized. In the parallel hybrid machine, the back-EMF fundamental amplitudes drastically drop, suggesting that the VPMs have already undergone partial demagnetization. By comparison, the series hybrid machine only shows a slight decrease in back-EMFs, indicating that the VPM working point is stable. A problem in VFM machines is the intentional demagnetization and re-magnetization of VPMs, which is examined. Since the CPMs naturally have the ability to assist in demagnetizing the VPMs, the demagnetization in the parallel hybrid machine is drastic, and a low -i_d current can almost totally demagnetize the VPMs. On the other hand, with the help of the CPMs, the back-EMFs in the series hybrid machine gradually decrease.

Furthermore, because of the magnetic saturations, the re-magnetizations in the two machines are always more difficult than the demagnetizations. In the series hybrid VFM machine, the CPM facilitates the re-magnetization of the VPM; however, because of the relatively thick VPMs in the case, a slightly higher current is needed to achieve the full re-magnetization. The output torque and terminal voltage can be computed by using the sweep in FE simulations to determine the flux linkages of the machines excited with different current combinations. Both machines are in the full forward magnetization state, and the same bus voltage (650 V) and phase current (236 A) limitations are used. It is visible that the hybrid VFM machines operating in parallel and series both present an extensive range of constant power speeds. Furthermore, in the low-speed range, the series machine's torque is significantly higher than that of its parallel counterpart. In the high-speed range, the series machine's power output is likewise greater. The main advantage of VFM machines is the continuous -i_d reduction during flux-weakening operation, which may increase the machine efficiency. Comparing the two hybrid VFM machines' efficiency performance is therefore crucial. The VFM machine's efficiency map is computed, where the FE method is used to sweep the copper and iron losses with varying currents and determine the optimal efficiency at each operation point. The various VPM magnetization states should be combined for optimal efficiency since the VPM's magnetization state will be controlled in the VFM machine to produce the proper PM flux, resulting in low copper loss and low iron loss. Thus, the efficiency maps of the two VFM machines running at various VPM magnetization states, the full forward state (K_m = 1), the nonmagnetic state (K_m = 0), and the full reverse state (K_m = -1), are all assessed. With regard to the two machines' efficiency maps across the entire torque-speed envelops at various VPM magnetization states, it is evident that the two machines' increased torque output and increased efficiencies within the low-speed high-torque region are both a result of the stronger VPMs. On the other hand, since -i_d components are reduced, the weaker VPMs gain from higher efficiencies in the high-speed region. In the meantime, it can be seen that the parallel hybrid machine has higher efficiencies during high-speed operation, while the series hybrid machine shows significantly higher torques and higher efficiencies during the low-speed region. The integrated optimum efficiency performance is then demonstrated by combining the efficiency maps of each machine's full forward and full reverse states. The full forward state of both machines always yields the higher torque output, while the low-speed, high-torque region has the highest efficiency. However, the efficiency in the high-speed low-torque region can be significantly enhanced, even though the torque output is sacrificed in the full reverse state because of the weak PM. As a result, it is advantageous to flexibly change the magnetization state at various operation regions, such as full magnetization during high-torque and partial magnetization during high-speed. Comparing the hybrid VFM machines in series and parallel reveals that the series machine is more efficient when operating at high torque, while the parallel machine is better at operating at high speed, although with a lower power output.To verify the predictions, a pair of parallel and series hybrid VFM prototype machines, shown in Fig. 3.21, are built and tested. The stator and windings of the two machines are identical, and the table in Fig. 3.22 lists the prototypes' primary design specifications. Prior to being fitted into the rotor, the VPMs are non-magnetized, but the CPMs are fully magnetized. The back-EMFs exhibit an important range of variation. The difference between the measured and FE-predicted back-EMFs after magnetization is found to be rather large, whereas the difference after demagnetization is minimal. This is because the VPMs can be fully demagnetized with a relatively low current, and demagnetization is simpler than re-magnetization in a parallel machine. On the contrary, since the available current in the test platform is limited by the inverter and the VPMs cannot be fully re-magnetized, the working point of VPM would locate on the minor hysteresis loop, which is more challenging to accurately predict. It can be concluded that the series hybrid magnet machine represents the most balanced solution, with better torque density, greater magnetic stability and superior overall performance compared to the parallel configuration, which remains simpler to control but less robust from a magnetic point of view.

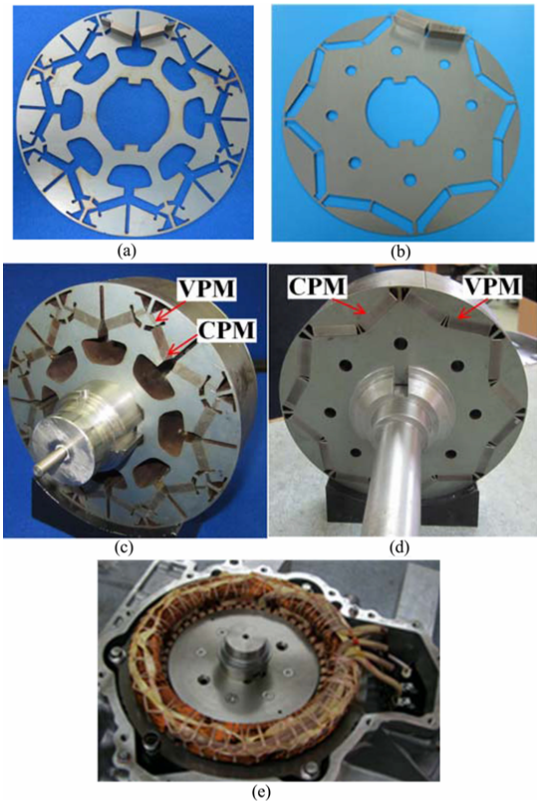

Figura 3.21: Prototypes of parallel and series hybrid VFM machines. (a) Paral lel hybrid lamination. (b) Series hybrid lamination. (c) Parallel hybrid rotor. (d) Series hybrid rotor. (e) Stator.
Source: [8]

Parameter	Series hybrid	Parallel hybrid
Phase number	3	3
Stator slot/rotor pole number	48/8	48/8
Axial length (mm)	50.8	50.8
Stator outer diameter (mm)	264	264
Stator inner diameter (mm)	161.9	161.9
Rotor outer diameter (mm)	160.44	160.44
Rotor inner diameter (mm)	68	68
Air-gap length (mm)	0.73	0.73
CPM thickness (mm)	6.5	6
CPM width (mm)	25	17.6
VPM thickness (mm)	7	2-2.5
VPM width (mm)	25	6.3
CPM B_r (T)	1.2	1.2
CPM H_c (kA/m)	915	915
VPM B_r (T)	1.14	1.14
VPM H_c (kA/m)	335	335
Steel grade	35H270	35H270
Number of turns per coil	11	11
Number of coils per phase	8	8
Rated current density (A/mm^2)	26.8	26.8

Figura 3.22: Key design parameters of parallel and series VFM machines.
Source: [8]

3.3.4 Comparison of end effect

End effects were compared in hybrid variable-flux permanent magnet (VFM) machines with series and parallel connections. This study is crucial to understanding the implications of these effects on machine performance, including parameters such as back EMF, torque, efficiency, and bearing safety. It is discovered that the series hybrid VFM machine experiences more severe end effects because of its asymmetric magnetic path, particularly the unipolar end leakage flux, whereas the parallel hybrid VFM machine always has relatively minor end effects. Furthermore, the VPM magnetization states have a notable impact on the end effect of the series VFM machines; the more the VPMs' magnetization level differs from the CPMs', the more severe the end effect. In fact, machines with various pole configurations, such as consequent-pole machines and hybrid-excited machines, can generally benefit from this conclusion.

3.4 Hybrid-Magnetic-Circuit VFM

An alternative hybrid magnetic circuit flux memory machine (HMC-VFMM) has been studied with the aim of improving efficiency and reliability for electric vehicle (EV) applications by combining the advantages of two existing types:

- Parallel type, which allows for a wide flux regulation range.
- Series type, which allows for excellent resistance to demagnetization under load.

The table in the Fig. 3.23 presents a qualitative comparison of the main features of conventional series and parallel VFMMs. Both two types of VFMMs can achieve satisfactory torque density due to the utilization of two sets of hybrid magnets, i.e., NdFeB and AlNiCo magnets. Meanwhile, a higher on-load demagnetization withstand capability, and a larger reluctance torque can be simultaneously obtained in the series structure. On the other hand, the parallel type shows a lower required maximum demagnetizing current level and a wider flux regulation range.

Types	Parallel	Series
Torque capability	High	High
Flux adjusting range	Wide	Narrow
Maximum demagnetizing current level	Low	High
Reluctance torque	No	Yes
High-speed power maintaining capability	Fair	High
Structure simplicity	Fair	Good
On-load demagnetization	Yes	No

Figura 3.23: Characteristics comparison of series- and parallel-type VFMMs. Source: [26]

3.4.1 HMC-VFMM Configuration and Variable Flux Principle

Figs. 3.24 and 3.25 show the machine configuration and the evolution of the topology, respectively. The dual-layer PM structure of the considered HMC design allows it to effectively combine the unique benefits of both parallel and series structures. The "U"-shaped hybrid magnet arrangement is used for the parallel branch. The spoke-type arrangement of the HCF PMs for the series branch creates a dual-layer series structure. Since the parallel/series magnetic circuits are made as a separate dual-layer configuration, the HMC design's parallel circuit has the ability to short-circuit most of the NdFeB magnetic fluxes inside the rotor core, giving it a wide range of flux adjustment.

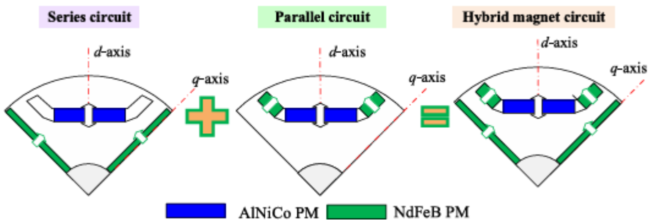

Figura 3.24: Topology evolution of considered HMC-VFMM.
Source: [26]

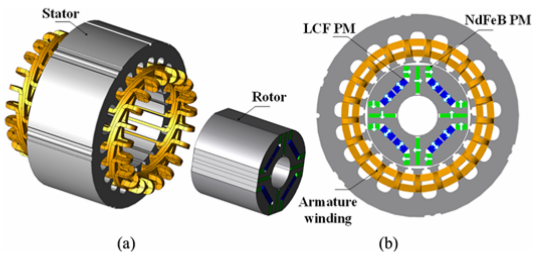

Figura 3.25: Considered HMC-VFMM. (a) Three-dimensional exploded view. (b) Cross-sectional view.
Source: [26]

Due to the dual-layer structure, the drawbacks of the high magnetizing current level and restricted flux regulation range of the series type are resolved as well. Besides, the existence of the series circuit branch in the HMC-VFMM permits a higher on-load demagnetization to withstand capability of LCF PMs due to the stabilizing effect of NdFeB PMs on the working point of the LCF PMs. In other words, the overload capability of the HMC-VFMM is further improved without unintended demagnetization. On the other hand, the unintended de magnetization can be also effectively prevented when a continuous negative d-axis current is applied for on-load maximum-torque-per-ampere operation of the considered HMC-VFMM. Therefore, the analyzed HMC design is advantageous to the online dynamic performance promotion as the peak torque of the machine increases. A brief current pulse with very little excitation copper loss can be used to successfully re-magnetize or demagnetize the LCF PMs. As a result, high efficiency can be sustained through a wide range of loads and speeds. It is discovered that the energy needed to change the magnetization state (MS) is comparatively low when compared to the energy loss needed to weaken the flux of an ordinary rare earth PM machine. However, even if the conventional loss (i.e., steady-state loss) decreases via the MS adjustment, the loss from magnetization current would result in larger net losses from the extremely frequent MS manipulation. In order to lower the overall energy losses, the MS operation's hysteresis control is used. When compared to the steady-state loss with a suitable control strategy, the energy needed to alter MS seems minimal. A simplified hysteresis model of the LCF PM, as shown in Fig. 3.26, can be used to illustrate the variable flux principle of the adopted HMC-VFMM. It is observable that the PM working point can be repeatedly adjusted between various recoil lines by applying either a re-magnetizing or demagnetizing current pulse because of the low coercivity and nonlinear hysteresis feature.

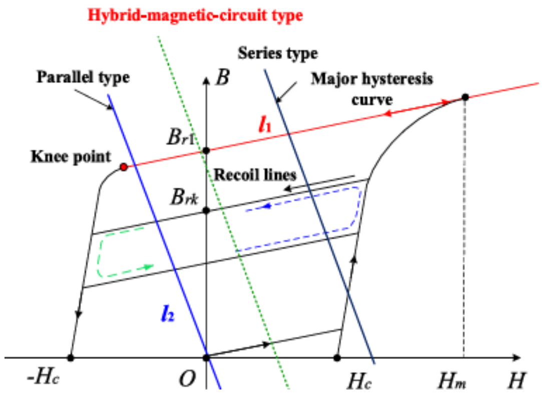

Figura 3.26: Simplified hysteresis model of the LCF PMs in three VFMMs. Source: [26]

This model assumes that all minor loops and the major hysteresis loops have different remanence B_{rk} values but the same coercive force H_c. The following is an expression for the collection of recoil lines designated with l_1:
$B = \mu_0 \mu_r H_m + B_{rk}$ where H_m is the strength of the positive magnetic field, B_{rk} is the corresponding k-th remanence of the sets of hysteresis loops, and μ_0 and μ_r are the vacuum permeability and the relative permeability of LCF PM, respectively. The ratio of B_{rk} to the remanence B_{r1} is known as an MS ratio, or k_{MS}:

$$k_{\text{MS}} = \frac{B_{rk}}{B_{r1}} \times 100\%, \qquad k = 1,2,3,\ldots$$

It goes without saying that as k_{MS} varies, the air-gap flux can be freely changed. As the MSs of LCF magnets approach the maximum and minimum, respectively, we define the "flux-enhanced" and "flux weakened" states. Since the LCF and HCF PMs are situated on two separate branches in the parallel case, the necessary magnetizing current magnitude and inverter rating are lowered. Given that the working point of the LCF PMs varies widely, the flux adjustment range may then be optimized to be sufficiently wide. In contrast to the other two cases, the parallel case's load line is located on the left, indicating that the LCF PM's operating point is nearer the knee point. Because of the armature reaction fields, the LCF PM is therefore vulnerable to the on-load demagnetization. The HCF magnet raises the working point of LCF PMs for the series type, which helps to stabilize the working point of the LCF PM, especially when operating under load. The presence of the NdFeB PM, however, raises the magnetic reluctance for circulating the d axis magnetizing MMF in the conventional series structure, which in turn causes the necessary demagnetizing current to increase. Furthermore, the strong flux-enhancing effect of the NdFeB PMs on the LCF PMs results in a relatively narrow flux regulation range. A better balance between the magnetizing and demagnetizing current amplitudes is made possible by the HMC design's load line, which is positioned between the two load lines of the previous two scenarios. In the meantime, the suggested HMC design has a larger flux regulation range than its standard series counterpart due to the parallel magnetic circuit. In the meantime, the LCF PMs can effectively withstand the unintentional demagnetization effect generated by the NdFeB PM and armature reaction fields thanks to the series magnetic circuit.

3.4.2 Design Methodology of the analyzed HMC-VFMM

As shown in Fig. 3.27, a simplified magnetic circuit model is developed to further emphasize the previously mentioned benefits of the considered HMC-VFMM. In particular, the magnetic reluctances of the iron cores are neglected for simplicity, and the magnetic circuits of conventional parallel and series structures are also modelled for reference. Since only the steady-state peak air-gap fluxes at various MSs are analytically predicted to reflect the torque capability and flux adjusting range, it should be noted that the magnetization process is actually not included in the magnetic circuit analysis. The considered HMC-VFMM without NdFeB magnets in either parallel or series branches can be used as a fair comparison for the series and parallel VFMMs. Since portions of the HCF magnets move through the air gap via the bypass paths on both sides of the LCF PMs, the dual-layer design for the series type can actually be considered as a quasi series structure. We can fairly compare the electromagnetic performance of the analyzed HMC-VFMM using the quasi-series VFMM design. Furthermore, this quasi-series design can lower the inverter rating and the necessary magnetizing current level, which are acknowledged as the main issues with the current series VFMMs. It is also possible to preserve the advantageous on-load demagnetization withstand capability. For the sake of simplicity, it should be noted that the dual-layer quasi-series structure is referred to as "series-type" in the analyses that follow. First, the air-gap fluxes $\Phi_{p\delta+}$ and $\Phi_{p\delta-}$ at the flux-enhanced and flux-weakened states can be formulated

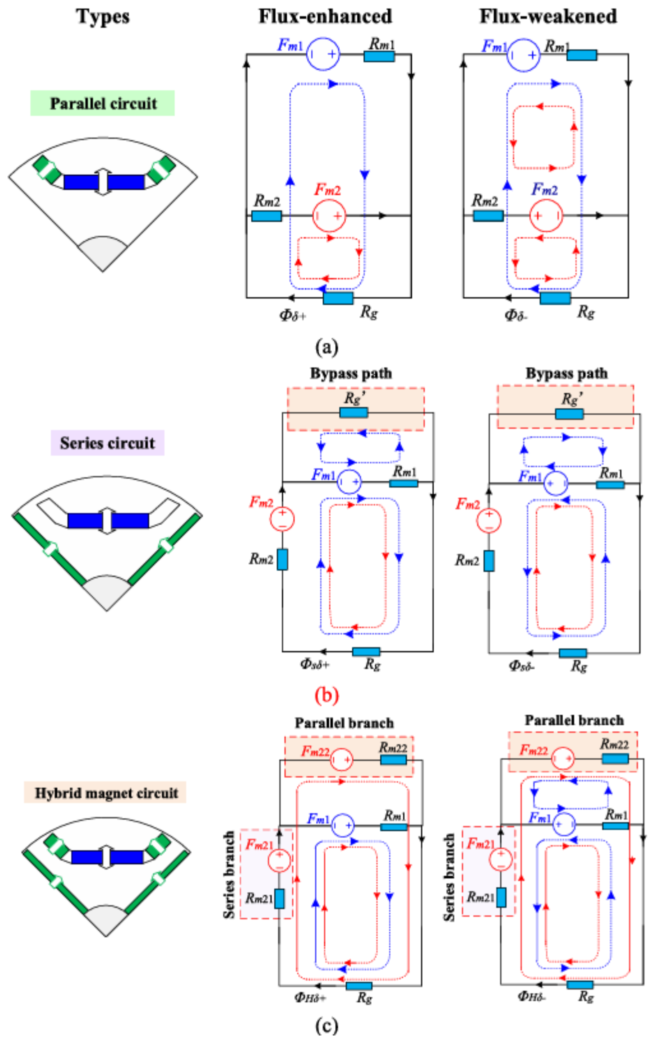

Figura 3.27: Simplified magnetic circuit models. (a) Parallel type. (b) Series type. (c) Considered HMC type.
Source: [26]

for the parallel case.

$$\begin{aligned}\Phi_{p\delta+} &= \frac{H_{c2} \cdot h_{m2} \cdot R_{m1} + H_{c1} \cdot h_{m1} \cdot R_{m2}}{R_g \cdot (R_{m1} + R_{m2}) + R_{m1} \cdot R_{m2}} \\ &= \frac{H_{c1} \cdot h_{m1}}{R_g} + \frac{\mu_{r2} \cdot \big(H_{c2} \cdot h_{m2} - H_{c1} \cdot h_{m1}\big) \cdot A_{m2}}{R_g \cdot \mu_{r2} \cdot h_{m1} + \mu_{r1} \cdot h_{m2} \cdot A_{m1}}\end{aligned} \tag{3.11}$$

$$\Phi_{p\delta-} = \frac{H_{c2}\, h_{m2}\, R_{m1} - H_{c1}\, h_{m1}\, R_{m2}}{R_g\, (R_{m1} + R_{m2}) + R_{m1}\, R_{m2}} \tag{3.12}$$

where R_g is the air-gap magnetic reluctance, h_{m1} and h_{m2} are the thicknesses of LCF and NdFeB PMs, respectively, and H_{c1} and H_{c2} are the coercive forces of LCF and NdFeB PMs, respectively. The corresponding peak open-circuit air-gap fluxes $\Phi_{p\delta+}$ and $\Phi_{p\delta-}$ at the flux-enhanced and flux-weakened states for the series type can be expressed similarly as follows:

$$\Phi_{s\delta+} = \frac{\frac{H_{c1}\cdot h_{m1}\cdot R_g}{R_g+R_{m1}} + H_{c2}\cdot h_{m2}}{R_g + \frac{R_{m1}\cdot R_g}{R_g+R_{m1}} + R_{m2}} \tag{3.13}$$

$$\Phi_{s\delta-} = \frac{\frac{H_{c1}\cdot h_{m1}\cdot R_g}{R_g+R_{m1}} - H_{c2}\cdot h_{m2}}{R_g + \frac{R_{m1}\cdot R_g}{R_g+R_{m1}} + R_{m2}} \tag{3.14}$$

However, the superposition method can be used to represent the open circuit peak air-gap fluxes $\Phi_{H\delta+}$ and $\Phi_{H\delta-}$ at the flux-enhanced and flux-weakened states for the considered HMC design:

$$\Phi_{H\delta+} = \frac{H_{c2}\cdot h_{m21}\cdot (R_{m1}+R_{m22}) + R_{m22}\cdot \Big(H_{c1}\cdot h_{m1} + H_{c2}\cdot h_{m22}\Big)}{R_{m21}\cdot R_{m22} + R_g\cdot R_{m22} + R_{m1}\cdot R_g + R_{m1}\cdot R_{m22} + R_{m1}\cdot R_{m21}} \tag{3.15}$$

$$\Phi_{H\delta-} = \frac{H_{c2}\cdot h_{m21}\cdot (R_{m1}+R_{m22}) + \Big(H_{c2}\cdot h_{m22} - H_{c1}\cdot h_{m1}\Big)\cdot R_{m22}}{R_{m21}\cdot R_{m22} + R_g\cdot R_{m22} + R_{m1}\cdot R_g + R_{m1}\cdot R_{m22} + R_{m1}\cdot R_{m21}} \tag{3.16}$$

where the magnetic reluctances of the NdFeB PM portions for the parallel and series branches are denoted by R_{m22} and R_{m21}, respectively. The ratio of the peak air-gap fluxes at the flux-enhanced and flux-weakened states, which can describe the air-gap flux control range, is known as the flux adjusting ratio, or α_{mag}.

$$\alpha_{\text{pmag}} = \frac{H_{c2}\,h_{m2}\,R_{m1} + H_{c1}\,h_{m1}\,R_{m2}}{H_{c2}\,h_{m2}\,R_{m1} - H_{c1}\,h_{m1}\,R_{m2}} = 1 + \frac{2}{\dfrac{H_{c2}\,\mu_{r2}\,A_{m2}}{H_{c1}\,\mu_{r1}\,A_{m1}} - 1} \tag{3.17}$$

$$\alpha_{\text{smag}} = \frac{\dfrac{H_{c1}\,h_{m1}\,R_g}{R_g+R_{m1}} + H_{c2}\,h_m 2}{\dfrac{H_{c1}\,h_{m1}\,R_g}{R_g+R_{m1}} - H_{c2}\,h_{m2}} = 1 + \frac{2\,H_{c2}\,h_{m2}}{\dfrac{H_{c1}\,h_{m1}\,R_g}{R_g+R_{m1}} - H_{c2}\,h_{m2}} \tag{3.18}$$

$$\begin{aligned}\alpha_{H\text{mag}} &= \frac{H_{c2}h_{m22}R_{m22} + H_{c2}h_{m21}R_{m1} + H_{c2}h_{m21}R_{m22} + H_{c1}h_{m1}R_{m22}}{H_{c2}h_{m22}R_{m22} + H_{c2}h_{m21}R_{m1} + H_{c2}h_{m21}R_{m22} - H_{c1}h_{m1}R_{m22}}\\ &= 1 + \frac{2}{H_{c2}\,(h_{m21}+h_{m22})\,H_{c1}h_{m1} + \left(\frac{H_{c2}\,\mu_{r2}A_{m22}}{H_{c1}\,\mu_{r1}A_{m1}}\right)\frac{h_{m21}}{h_{m22}} - 1}\end{aligned} \tag{3.19}$$

where the cross-sectional areas of the LCF and NdFeB PMs are denoted by A_{m1} and A_{m2}, respectively. The thicknesses of the NdFeB PM sections on the series and parallel branches are denoted by h_{m21} and h_{m22}, respectively, while the relative permeabilities of the LCF and NdFeB PMs are represented by μ_{r1} and μ_{r1}. The cross-sectional regions of the NdFeB PM portions on the parallel and series branches are denoted by A_{m21} and A_{m22}, respectively. From (3.11) to (3.18), it can be determined that the current parallel and series VFMMs have a design trade-off between torque capability and flux adjusting range. The normalized maximum air-gap flux and flux adjusting ratio variations with the magnet cross-sectional ratio (A_{m2}/A_{m1}) and the thickness ratio (h_{m2}/h_{m1}) of the parallel and series VFMMs are displayed in Fig. 3.28 along with the analytical and FE-predicted variations. The key performance parameters are mostly determined by PM cross sectional and thickness ratios for the parallel and series cases, respectively, according to the satisfactory agreement between the analytical and FE results. However, (3.15), (3.16), and (3.19) show that the HMC design can obtain a larger design space by properly designing multiple variables, such as the PM cross-sectional and thickness ratios (h_{m21}/h_{m22}, A_{m21}/A_{m22}, and h_{m22}/h_{m21}), rather than just one in either parallel or series type. Compared to its series/parallel counterparts, it is evident that the suggested HMC design is better able to balance the trade-offs between the torque capability and the flux adjusting ratio. This further demonstrates the previously stated benefit of the suggested HMC structure. The efficacy of the analytical model mentioned before is confirmed by the overall good agreement between the FE and analytical results. The on-load demagnetization effect is intended to be mitigated by the triangular q-axis barriers. It is visible that the enhanced design's working point level is higher than the original's. The operating point variations at the LCF PM's central point under an intermediate on-load operation also show this. It suggests that the enhanced design can successfully sustain the LCF PM's MS during load operation. This is primarily due to the barrier design's ability to successfully decrease the cross-coupling effect between LCF PMs and armature fields.The following two points illustrate how the q-axis barriers reduce the cross-coupling effect for the considered HMC-VFMM:
1) Saturation caused by the q-axis flux has a smaller impact on the magnet flux.
2) Without significantly reducing the magnet flux, the peak torque can be increased further.
Because of the cross-coupling saturation effect produced by the q-axis current, portions of the LCF PMs are considerably demagnetized in the HMC-VFMM case without q-axis barriers. With the limitations of the previously optimized magnet sizing ratios and a rated current density of 6.5 A/mm^2, the design parameters of the studied HMC-VFMM are globally optimized using a multi-objective genetic algorithm. The lowest LCF PM working point (BLCF) greater than 0.7 for the on-load demagnetization prevention and the maximum average torque (T_{ave}) at the

flux enhanced state are the optimization goals; the weighted factors for these are 1.0 and 0.5, respectively.

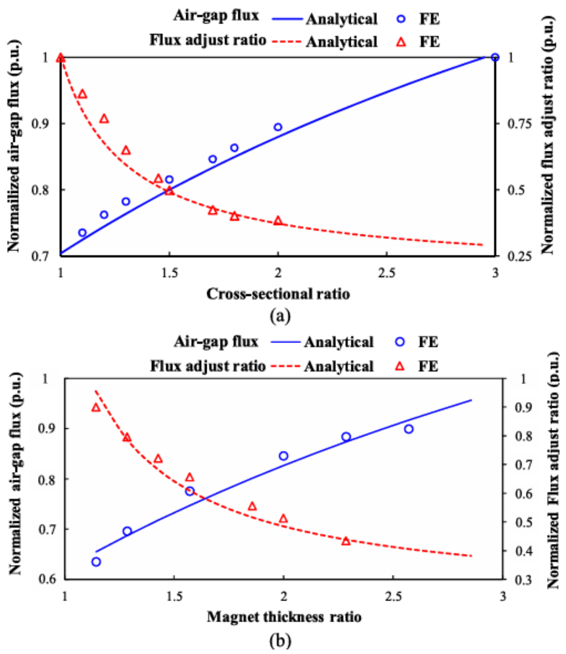

Figura 3.28: Comparison of FE and analytically predicted normalized peak air-gap flux and flux adjusting ratio. (a) Parallel type. (b) Series type.
Source: [26]

3.4.3 Electromagnetic Performance Evaluation

The electromagnetic properties of the considered HMC-VFMM are compared with those of conventional parallel and series cases in order to verify its benefits and validity. The three VFMMs have the same stator-slot/rotor-pole numbers, winding configuration, total magnet usage, etc. for a fair comparison. The main design parameters of the three investigated VFMMs are optimized in order to balance the trade-off of the torque capability and flux regulation range, as tabulated in Fig. 3.29. It should be mentioned that compared to the series and HMC cases, the peak demagnetizing current level for the parallel structure is substantially lower. Its low magnetic reluctance for the d-axis fluxes and lowest working point of LCF PM are the causes of this. However, the three machines' necessary peak re-magnetizing currents are comparable. This is because, in the series and HMC scenarios, the NdFeB magnets' flux-enhancing effect on the LCF magnets would reduce the necessary peak re-magnetizing current. Fig. 3.30 illustrates the open-circuit field distributions under various MSs. As expected, the parallel VFMM shows the largest flux regulation range, followed by the considered HMC-VFMM.

Items	Parallel	Series	HMC
Rated power (kW)	1.1	1.0	1.2
Rated speed (r/min)		1500	
Outer diameter of stator (mm)		122	
Inner diameter of stator (mm)		63.5	
Stator tooth width (mm)		4.8	
Air-gap length (mm)		0.35	
Active stack length (mm)		55	
HCF PM grade		NdFeB N35SH	
LCF PM grade		AlNiCo 9	
HCF/LCF PM coercivity (kA/m)		915/112	
HCF/LCF PM remanence (T)		1.2/1.0	
MS range (T)	-0.45~0.83	0.20~0.97	0~0.92
Peak magnetizing current (A)	42	48	45
Peak demagnetizing current (A)	-15	-30	-27
Steel grade		35CS440	
Armature winding turns per phase		210	
Rated current (A)		7.5	
DC-link voltage U_{dc} (V)		200	

Figura 3.29: Key design specifications of series, parallel and analyzed HCM-VFMM.
Source: [26]

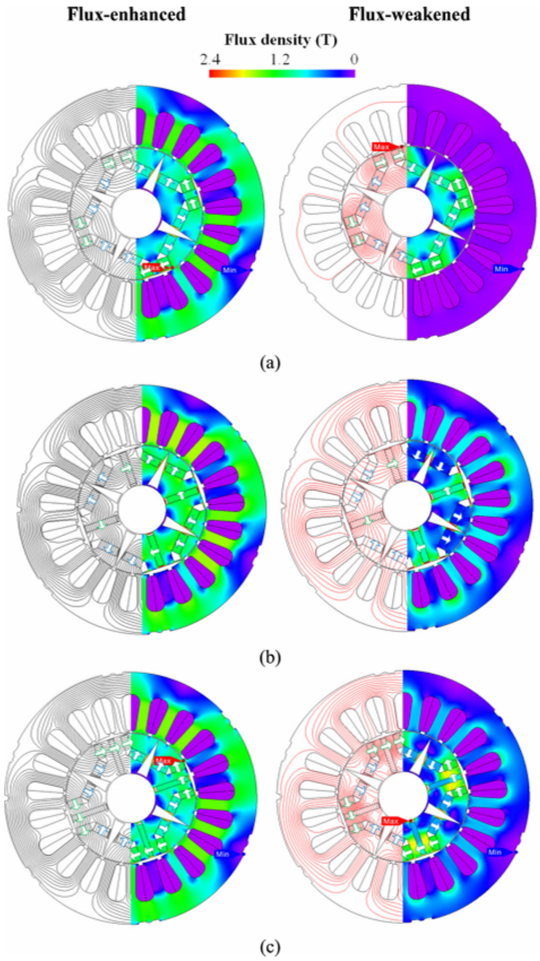

Figura 3.30: : Open-circuit field distributions under different MSs. (a) Parallel VFMM. (b) Series VFMM. (c) Analyzed HMC-VFMM.
Source: [26]

The series structure, which benefits from the dual-layer design, shows a required full re-magnetizing current level that is comparable to both the parallel case and the considered HMC design. Additionally, as was previously mentioned, the parallel case exhibits the lowest fully demagnetizing current. Because the load line of the HMC case is intended to be between those of the series and parallel VFMMs, the analyzed HMC-VFMM exhibits a slightly lower fully demagnetizing current level than the series case. The torque–current angle curves at the flux-enhanced state are examined previously in order to select an appropriate current control strategy that will optimize the torque capability. The saliency ratios of the HMC and series designs are similar; however, the parallel case exhibits a negligible reluctance torque, primarily because of the substantial cross-coupling demagnetization effect in the LCF PMs. Compared to its series and parallel counterparts, the HMC-VFMM offers average torques that are 22.3% and 25.7% higher, respectively, along with torque ripples that are 56.52% and 65.70% lower. It should be mentioned that the significant unintentional demagnetization of LCF PM during the on-load operation is the primary cause of the torque decrease in the parallel case. Furthermore, because of the nonlinear hysteresis property, the coverage process in FE software takes a quite long time because of the more extreme fluctuation of the working points of LCF PMs in the parallel structure. Under rated-load operation, the three VFMMs' on-load demagnetization with stand capability is investigated. It is evident that the parallel VFMM experiences considerable unintentional demagnetization. Despite having a slightly lower working point than its series counterpart, the analyzed HMC can effectively maintain the MS under load. With regard to losses, regardless of the MSs, the parallel VFMM exhibits greater loss than its series and HMC counterparts. This is mostly explained by the spoke-type PMs' absence in the parallel structure as a q-axis barrier, which helps to lower the low-order armature harmonics and, consequently, the eddy-current loss. All things considered, it demonstrates that the three machines can all operate within a comparatively wide operating range while increasing their efficiency through the use of MS manipulation control. Furthermore, because of its highest torque capability, the HMC case shows the largest high-efficiency region and the highest peak efficiency independent of MSs. The above theoretical and FE analyses are validated by manufacturing and testing a 21-slot/4-pole HMC-VFMM prototype. As expected, it is observable that the HMC design can achieve a good flux regulation capability. The primary cause of the small discrepancy between the measured and FE results is that the FE analyses don't take mechanical tolerance or end effects into account. With the help of MS manipulation control, the considered HMC-VFMM can efficiently increase the speed range. Overall, the theoretical analyses are confirmed by a good agreement between the FE predicted and test results. It can be concluded that the considered HMC-VFMM compromises between parallel and series solutions. It offers a better combination of flux regulation, torque quality, efficiency, and resistance to demagnetization under load.

3.5 Hybrid-PM Switched-Flux Memory Machine

Generally speaking, Memory Machines can be divided into two types based on the winding patterns that supply current pulses: alternating current (ac) and direct current (dc) magnetized types. Ostovic was the first to propose AC-magnetized MM. An interior PM (IPM) machine uses aluminium-nickel-cobalt (Al-Ni-Co) trapezoidal spoke-type magnets, and flux barriers are used to mitigate the negative effect of the q-axis armature reaction on the PMs. Furthermore, a number of "flux-intensifying" designs have been set to enable the maintenance of the on-load magnetization state because of the reversed saliency. The inverter rating and full magnetizing current were decreased by using fractional-slot winding configurations. However, low-coercivity magnets for ac-magnetized MM are typically vulnerable to armature reaction, and their industrial applicability is unavoidably compromised by the increased requirements for current vector control. However, dc-magnetized MM, which uses extra dc coils to magnetize and demagnetize the low-coercivity magnets, was suggested based on the extensively studied PM machines with PM on the stator. In order to make online magnetization control easier, the corresponding doubly salient (DS) MM was published. Nevertheless, it has a significant torque ripple by nature, which is undesirable for EV/HEV operating conditions. In order to create an alternative series of switched-flux MM (SFMM), the switched-flux topologies were then applied to MM. Single PM arrangements that were either surface mounted or internally embedded were analyzed. There are multiple benefits to SFMMs, such as high rotor robustness, simple thermal dissipation, and essentially sinusoidal back electromotive force (EMF) that is perfect for brushless AC (BLAC) operation. In contrast to their DS counterpart, SFMMs exhibit a higher torque density and a lower torque ripple. However, despite having a sufficiently large speed range, the previously reported stator-excited MMs employing a single low-coercivity magnet frequently have a relatively low torque density. In order to solve the issues mentioned previously, the hybrid PM design was expanded to either DSMM or SFMM. Unbalanced force is unavoidable in the 6/5-stator/rotor pole scenario, which is the only one covered by the studies that are currently available. Furthermore, by concurrently doubling the stator and rotor numbers, this drawback can be removed. As a result, a 12-stator pole hybrid-PM SFMM (HPM-SFMM) design theory and electromagnetic performance are taken into consideration. The torque enhancement of Nd-Fe-B PM and the flux variability of Al-Ni-Co PM work in tandem in this machine design. From a geometric perspective, the considered machine can be viewed as a hybrid of the single-PM SFMM (Fig.3.31(b)) and the conventional SFPM machine (Fig. 3.31(a)). Its topology is illustrated in Figs. 3.31(c) and (d).

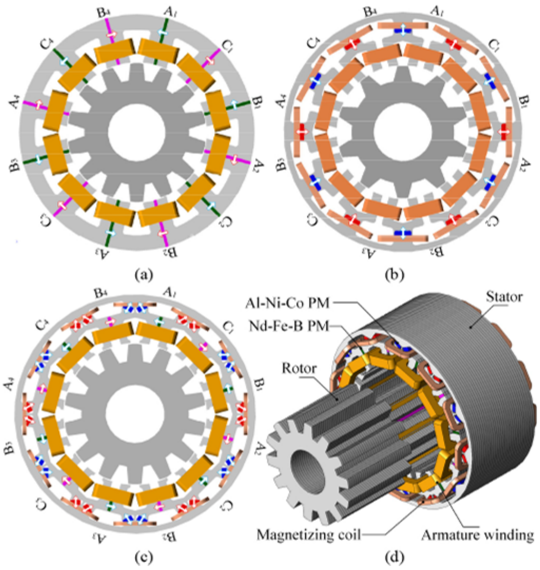

Figura 3.31: Illustration of conventional SFPM machine and considered SFMMs. (a) Conventional SFPM machine. (b) Single-PM SFMM. (c) Cross-section and (d) 3-D schematic of HPM-SFMM.
Source: [28]

3.5.1 Machine Design and Working Mechanism

The suggested HPM-SFMM is composed of a usual SFPM machine with extra "V"-shaped Al-Ni-Co PM poles and an outer stator yoke layer, as shown in Fig. 3.31. This permits the effective flux concentration. In the meantime, a large torque capability and an ample speed range can be achieved by expanding the cross-sectional magnet area within a constrained circumference. Adjacent "U"-shaped stator iron segments partially enclose circumferentially magnetized Nd-Fe-B PMs, while the magnetizing coils are wound on Al-Ni-Co magnet poles. As a result, the magnetic saturation that causes high torque ripple and magnet eddy-current loss is greatly reduced, and the use of rare-earth magnets can be limited to deal with the costly and scarce rare-earth material. More significantly, it is possible to prevent the undesired irreversible demagnetization and performance degradation of Al-Ni-Co PMs caused by Nd-Fe-B PM. The following is a summary of the other unique aspects of the considered HPM-SFMM:

- The robustness of the mechanical system. The rotor is simple to build and solid, and all excitation sources are situated on the stator, which leads to efficient thermal control.

- When Nd-Fe-B and Al-Ni-Co PMs share the same magnetization directions, the hybrid magnet arrangement allows for the achievement of a high torque capability at low speeds. To enable the desired flux-weakening performance, or the effective extension of the constant power operating range within the constraints of the inverter power rating, Al-Ni-Co PMs are reversely demagnetized for high-speed operation.
- The armature and PM fields have parallel magnetic pathways. This advantage enables the Al-Ni-Co magnet to withstand high loads and good demagnetization, both of which are essential for MM design.
- Online flux control with high performance. In order to eliminate excitation loss and simplify online magnetization control, current pulses are applied in the auxiliary magnetizing winding in a matter of milliseconds. The polarity and magnitude of PM fluxes interacting with the armature vary as a result of the rotor's rotational alignment change with the stator. As a result, sinusoidal back EMF will be generated. The term "positive-magnetization" describes how the Nd-Fe-B PMs and Al-Ni-Co PMs have the same magnetization directions. On the other hand, the "negative-magnetization" effect is made possible by the Al-Ni-Co fluxes in the stator core, which will significantly short circuit the Nd-Fe-B fluxes.

3.5.2 Determining the Optimal Stator-Rotor Pole Combination

The distribution factor k_d of the stator windings can be determined using a formula similar to that for conventional SFPM machines:

$$k_d = \frac{\sin(Qk\alpha/2)}{Q\sin(k\alpha/2)} \tag{3.20}$$

The distribution factor k_d of the stator windings can be determined using a formula where k is the order of the EMF harmonic, α is the angle between two adjacent vectors, and Q is the number of the least EMF vectors per phase. Furthermore, the coil pitch factor can be written as follows as a function of stator/rotor pole numbers (N_s/N_r):

$$k_p = \cos\left[\pi k\left(\frac{N_r}{N_s} - 1\right)\right] \tag{3.21}$$

For the analyzed HPM-SFMM, the stator pole number design consideration is taken into account in advance. The stator/rotor pole numbers (N_s/N_r) for the three-phase all-pole-wound HPM-SFMMs should be controlled by the following in order to achieve symmetrical back EMF:

$$\frac{N_s}{\mathrm{HCF}(N_s, N_r)} = 6j \tag{3.22}$$

where j is a positive integer and HCF stands for the highest common factor. The stator-PM configuration requires that Ns be an even number, so it can be designed as multiples of 6, usually 6, 12, 18, 24, and so forth. In the meantime, the stator has two sets of PMs and windings (18, 24). Because of their congested stator spaces and unavoidable magnetic saturation, other stator pole configurations are not included in the analysis that follows. Consequently, the corresponding winding factor kw, distribution factor, and fundamental pitch factor for the presented HPM-SFMMs with 6 and 12 stator poles are given in the table in the Fig. 3.32. It is evident that when Nr is close to Ns, the winding factor is at its highest. Additionally, the 6/5 and 6/7-pole machines invariably exhibit an unbalanced magnetic force, which leads to vibration and acoustic issues. Therefore, the 12-stator pole structures are the primary focus. In order to achieve a design trade-off between torque and flux adjustability, as will be discussed later, the design parameters are globally optimized, subject to the limitations of fixed copper loss (200 W) and preoptimized PM cross-sectional ratio. Just the magnet dimensions optimization process is shown for simplicity's sake. As a result, 12-stator pole HPM-SFMMs with 10-, 11-, 13-, and 14-rotor poles are chosen and their electromagnetic performance compared.

N_r		2	4	5	7	8	10
N_s=6	k_p	0.5	0.5	0.87	0.87	0.5	0.5
	k_d	1	1	1	1	1	1
	k_w	0.5	0.5	0.87	0.87	0.5	0.5
N_r		8	10	11	13	14	16
N_s=12	k_p	0.5	0.87	0.97	0.97	0.87	0.5
	k_d	1	1	0.97	0.97	1	1
	k_w	0.5	0.87	0.94	0.94	0.87	0.5

Figura 3.32: Winding factors of 6- and12-stator pole HPM-SFMMS for different rotor pole numbers.
Source: [28]

The frozen permeability method (FPM), which accounts for the cross-coupling effect and magnetic saturation, predicts the armature-reaction field distributions with respect to various rotor poles. The 14-rotor-pole machine's Al-Ni-Co magnets are shown to have the best irreversible demagnetization withstand capability from armature fields, which is advantageous for online magnetization control. Similar back EMFs with the largest amplitudes and the sinusoidal level are seen in machines with 13- and 14-rotor poles. The three magnetization states, positive magnetization (fully re-magnetizing Al-Ni-Co PMs), zero magnetization (fully demagnetizing Al-Ni-Co PMs), and negative magnetization (reversely re-magnetizing Al-Ni-Co PMs), are categorized based on the current pulse amplitudes. The 13-rotor-pole machine's winding factor (0.94) is greater than the 14-rotor-pole machine's (0.87) for 12-pole stator machines with an all-pole-wound winding configuration. The 13-rotor-pole machine has a slightly higher flux linkage as a result. However, the 14-rotor pole one has a higher electric frequency (proportional to the number of rotor poles). As a result, the torque capabilities of the 13- and 14-rotor pole configurations are comparable to and higher than those of the others. Furthermore, the 12/13-pole machine will have an unbalanced magnetic force. For the upcoming research and prototype construction, the HPM-SFMM with a stator/rotor pole configuration of 12/14 is therefore preferred. Because of the severe localized magnetic saturations and doubly saliency nature, the high torque ripple persists. To reduce torque ripple, the stator tooth tips and rotor-pole chamfering are combined. The rotor chamfering radius is denoted by R_r, and the stator tooth-tip width by l_t. The parameters with l_t and R_r of "20 +3" are used in this instance. The torque ripples are effectively reduced by the combination method. Compared to tooth tip or chamfering schemes, the machines with combined geometric changes have a higher torque capability. In order to minimize torque ripple without drastically compromising the torque output, the combined variations are used for prototype fabrication.

3.5.3 Analysis of Hybrid PM Configurations

It is essential to correctly select the Al-Ni-Co grade, because its operating point must remain stable even in the presence of the fields generated by the Nd-Fe-B magnets. Grades 5, 8, and 9 have been analyzed, and grade 9 turns out to be the most suitable: in fact, it offers good resistance to demagnetization and contributes significantly to torque production. Lower grades (e.g., 5) have too low coercivity and risk reverse re-magnetization by the Nd-Fe-B magnets. The combined use of Nd-Fe-B (strong but rigid) and Al-Ni-Co (weak but controllable) can lead to stator iron saturation, especially with overly powerful magnets. A design compromise is therefore required between high torque and flux control capability. Through the analysis of equivalent magnetic circuits (EMC) and the flux in the air gap in different magnetization states (positive, zero, negative), it is shown that flux control depends primarily on the ratio between the areas and coercivities of the two magnets. The electromagnetic torque increases as the cross-section of the Nd-Fe-B increases, but this reduces the flux control capability. The optimal hybridization ratio is therefore defined:

$$k_m = \frac{A_{m2}}{A_{m1}} \tag{3.23}$$

(A_{m2} and A_{m1} are the cross-sectional areas of Al-Ni-Co and Nd-Fe-B) with an optimal value of approximately 0.85, which ensures the best balance between torque and flux flexibility. Finite element analysis (FEA) simulations confirm the analytical results, with small discrepancies due to iron reluctance and saturation effects not considered in the EMC models. The magnetization slot size (A_{ms}) and the required magnetomotive force (F_{mag}) to ensure effective re-magnetization of the Al-Ni-Co are also determined, considering the pulse current density (J_{ms} $\approx$ 50 A/mm^2). This calculation results in optimal lengths of approximately 8.4 mm for Al-Ni-Co and 7.2 mm for Nd-Fe-B, with a “V” geometry to increase the effective magnetic area and reduce converter requirements. To avoid reverse re-magnetization of Al-Ni-Co during operation under load, the following constraint must be respected:

$$F_{m2} = H_{c2}h_{m2} - 2H_{c1}h_{m1} \leq 2k_{\text{intrinsic}}H_{c1}h_{m1} \tag{3.24}$$

from which this relation is obtained:

$$h_{m2} \leq 0.68\, h_{m1} \tag{3.25}$$

Optimization shows that increasing thickness improves torque but affects flux control due to magnetic saturation. Furthermore, excessive use of Nd-Fe-B increases costs and causes over-demagnetization of Al-Ni-Co magnets. The analysis leads to an optimal value of thickness $h_{m1} \approx 4\,\text{mm}$ and $h_{m2} \approx 2.5\,\text{mm}$, which provides a good compromise between average torque, efficiency, and control range. Simulations confirm that excessive Nd-Fe-B thickness generates irreversible cross-demagnetization, limiting the contribution of Al-Ni-Co to torque production, as Fig. 3.33 shows. The trend of the demagnetization ratio and flux density demonstrates that moderate use of rare earth elements ensures the best dynamic performance and magnetic stability.

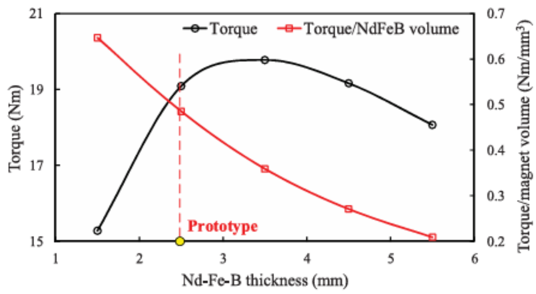

Figura 3.33: Variations of average torque and torque against rare-earth volume with the Nd-Fe-B thickness.
Source: [28]

3.5.4 Performance analysis

The applied current pulses allow for flexible adjustment of the air-gap flux density. The abundant field harmonics in the considered HPM-SFMM, directly contributed to the torque production, making it a flux-modulation machine. The magnetization control allows for flexible adjustment of the back EMFs, resulting in a high-speed flux-weakening capability that is satisfactory. Specifically, the speed range can be efficiently increased while staying within the inverter voltage constraints. Furthermore, regardless of the magnetization states, the back EMFs essentially stay sinusoidal, which is perfect for BLAC operation. The HPM-SFMM's torque profiles change sinusoidally with current angle; that is, the maximum torque is achievable at nearly zero current angle. As a result, the HPM-SFMM can be controlled with $I_d = 0$. Under the negative magnetization state, the HPM one exhibits a maximum torque ripple rate of 12.5%, which is suitable for EV/HEV applications. By altering the magnetization states of Al-Ni-Co PMs, the HPM-SFMM demonstrates exceptional flux adjustable capability. Since the circulating short-circuited flux weakens the magnetic saturation in the rotor core and reduces the fluctuation in iron flux density in the stator fields, lowering the magnetization levels of Al–Ni–Co magnets can significantly reduce iron loss. By lowering iron losses, the magnetization control increases the overall efficiency. It is evident that by combining the best efficiency features under each magnetization state, the high-efficiency operation can be extended with a large range of speeds and loads. The zero- and negative-magnetization states are advantageous for constant-power operation with the minimized iron losses, which are typically the dominant loss component at high-speed regions, while the positive magnetizing operation is preferred for constant-torque operation to obtain high efficiency. Therefore, it is feasible to increase HPM-SFMM efficiency over an extended operating range. A 12/14-stator/rotor pole HPM-SFMM has been prototyped and tested in order to verify the FE predictions. Experimental measurements of back-EMF and magnetization behavior are consistent with FE simulations. The experiments show stable magnetization transitions and currents up to 17.5 A required for full magnetization. However, the cost can be reduced without using comparatively expensive power converters by using a capacitor-based magnetization control circuit. It can be concluded that:

- The considered HPM-SFMM combines the advantages of Nd-Fe-B magnets (high torque) and Al-Ni-Co (tunable flux).
- It achieves an excellent compromise between torque, speed range, and efficiency.
- It exhibits excellent flux control capability, thermal robustness, and low excitation losses.
- It is a promising solution for EV/HEV traction motors, with superior performance compared to single-magnet machines.
- Future work will include dynamic study and the use of DC magnetizing coils as continuous excitation sources to further increase torque.

3.5.5 Flux-Concentrated External-Rotor Switched Flux Memory Machines

Permanent magnet (PM) machines with external rotors (ER) are well known for being a preferred alternative for in-wheel automotive propulsion. They gain from the drive stiffness, low rotating inertia, high torque density, and easy direct coupling with rotating tires. Additionally, the torque enhancement benefits from the high stator space utilization. Memory machines were added to the switched flux (SF) topologies. Similar as conventional SFPM machines, the unique features, such as sinusoidal back-EMF and exceptional armature demagnetization withstand capability, remain. The SF-HMMM topologies with spoke-PM ER and "U"-shaped PM IR configurations are shown in Fig. 3.34. It is evident that in the "IR" case, the crowded stator naturally lowers the split ratio, whereas in the "ER" case, the ER design allows for adequate stator space.

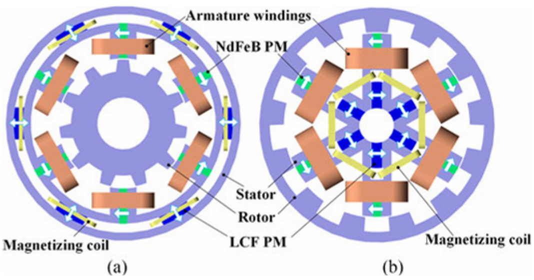

Figura 3.34: Illustrations of SF-HMMMs with (a) IR and (b) ER configurations. Source: [39]

The aim is to identify the optimal N_s/N_r combination that maximizes the electromagnetic torque and improves the efficiency in the use of permanent magnets, also taking into account the slot-opening ratio. The following is a definition of the slot opening to NdFeB magnet thickness α_{sm} ratio:

$$\alpha_{sm} = \frac{\tau_{so}}{h_{m1}} \tag{3.26}$$

where τ_{so} and hm1 stand for the slot opening width and NdFeB thickness, respectively. For ER-SFHMMMs, there are several possible stator/rotor pole number (N_s/N_r) combinations. In this case, the 6-stator pole machines are taken into consideration as a unit model for further research. The variable magnetic permeance between the stator tooth and the rotor pole is expressed by a simplified harmonic function that takes into account only the first dominant components, neglecting the higher harmonics. When the rotor is aligned with the d-axis, the no-load flux per phase (Φ_a) and the torque coefficient (k_t) are analytically deduced as functions of the number of rotor poles and the geometric parameters of the machine:

$$k_T \propto N_r\ k \ = \ N_r N_w \left(\left(\frac{P_{sr3}}{P_{sr3}+P_{sr4}}\right) - \left(\frac{P_{sro2}}{P_{sri1}+P_{sr2}}\right)\right) \tag{3.28}$$

Na = number of turns per phase,
k_w = winding factor,
P_{sr} = stator-rotor permeance components.

Among the various N_s/N_r combinations analyzed, the machine with 6 stator poles and 19 rotor poles was found to have: the highest torque density, the best torque-to-magnet mass ratio, and the highest efficiency in using permanent magnets. Fig. 3.35 illustrates the simplified equivalent magnetic circuits at various magnetization states. The ratio of the cross-sectional areas of the two magnets is known as the magnet hybridizing ratio, or k_{pm}:

$$k_{\mathrm{pm}} = \frac{l_{m1}}{l_{m2}} \tag{3.29}$$

where, l_{m1} and l_{m2} represent the NdFeB and LCF magnets' respective cross-sectional lengths. As in the earlier research, the flux-adjusting ratio β_m (which is the ratio of the maximum air-gap flux $\Phi_{\delta+}$ to the minimum $\Phi_{\delta-}$) and the maximum air-gap flux $\Phi_{\delta+}$ interfere.

It is demonstrated that a satisfactory performance trade-off can be achieved by achieving the ideal value of kpm of about 1.6. One of the main concerns is the irreversible demagnetization of LCF PMs produced by Nd-Fe-B PMs. Therefore, it is important to carefully design the LCF magnet's thickness to avoid this negative effect. This demagnetization behaviour is quantified using a coefficient k_{DE}, which is defined as follows:

$$k_{\mathrm{DE}} \ = \ \frac{B_{\mathrm{rp}} - B_{\mathrm{knee}}}{B_{\mathrm{knee}}} \times 100\% \tag{3.30}$$

where B_{knee} is the kneepoint's flux density and B_{rp} is the LCF PM's operating point. To effectively withstand the demagnetization risk, the ideal thickness of 2.5 mm can be obtained. To achieve adequate rotor saliency and lower magnetic saturation, the split ratio, that is, the ratio of the stator outer radius to the rotor outer radius, is set at 0.86. The electromagnetic properties of the presented spoke-type machine (see Fig. 3.36) and the "U"- shaped baseline machine are examined. With the exception of the armature turns per phase, which are caused by the same copper loss and a different slot area, the two machines have the same major geometric parameters and magnet usage. The following analyses are conducted using the same copper loss of 30W for fair comparison. The mechanical aspects should be taken into account because the rotor is a cupped structure. The rotor and end caps can be fixed together using metallic sticks or screws, which can offer some mechanical strength. As a result, the prototype can withstand some extreme operating circumstances. A rotating accessory shaft can be attached to the end cover in the interim. However, the mechanical fixation of the stator seems to be relatively simple, despite the stator lamination appearing to be rather complex. The convenience of PM magnetization, which is unaffected by rotor positioning, is brought about by the PMs' placement on the stator.

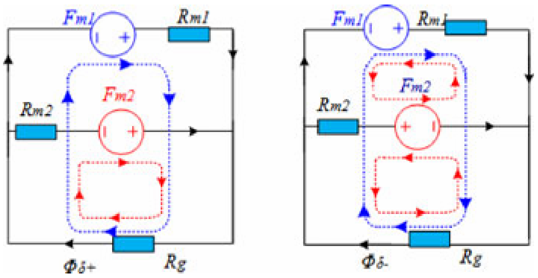

Figura 3.35: Simplified magnetic circuits. (a)Flux-enhanced.
(b)Flux-weakened.
Source: [39]

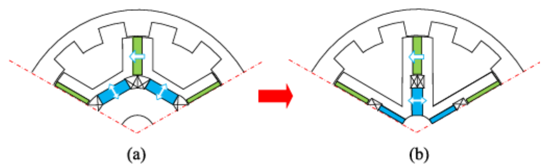

Figura 3.36: ER structures.
(a) "U"-shaped design (baseline).
(b) Spoke design.
Source: [39]

The magnetizing coil's self-inductance smoothly varies with the rotor position, demonstrating this. Furthermore, the PM magnetization current pulses are only energized for a few milliseconds. The actual magnetizing current density can therefore be designed at a relatively high level, resulting in a less stringent requirement for each magnetizing coil's wire radius. Actually, to permit a high enough transient current, a magnetizing circuit based on capacitor charging can be employed. The magnetization states can be categorized as flux-enhanced (+8000 A · turns), flux-weakened (-8600 A), or zero magnetized (-3200 or +5400 A · turns) based on the ampere turns per magnetizing coil. The effective flux-concentration is primarily responsible for the improved flux-adjusting capability of the considered design. Furthermore, the larger armature slot area in this design allows for the observation of higher magnitudes at the flux enhanced state. The two machines' on-load torque performance is computed with a 30W rated copper loss constraint. Because of the unity saliency ratio, the considered machines operate appropriately at brushless AC operation and zero d-axis current control. Under flux-enhanced conditions, this machine can produce 9.3% more torque than its baseline counterpart. It is evident that by combining various magnetization states at various speeds, the considered machine can provide extended high efficiency operation over a wide speed range. Additionally, both topologies seem to have minimal torque ripple, which is advantageous for cruising. It should be noted that the copper loss in the magnetizing coil can be neglected because the coils are only energized for a few milliseconds. Here, natural air cooling is used, and the end positions experience the highest winding temperature, which can reach up to 65.2 °C. The area surrounding the teeth is the hottest spot in the rotor, but overall, the temperature distribution is uniform, ranging from 35.6 to 39.4 °C. The joints with the shaft and air gap have the lowest temperature in the stator, which is about 45 °C. Better cooling methods can be used to improve the thermal condition because the PMs are on the stator. It can be concluded that this alternative solution spoke-type ER-SF-HMMM:

- increases torque by 9.3% compared to the conventional model
- maintains high efficiency and low torque ripple
- allows for efficient flux regulation without continuous losses
- is mechanically robust and easy to magnetize
- It offers a promising solution for direct-drive motors in electric vehicles (EVs), thanks to its high efficiency, wide speed range, and low magnet cost.

3.5.6 Fault Tolerant FSMM with Highly Flux-Controllability

Because of increased PM utilization and the flux-focusing effect brought on by spoke-type PM arrangements, FSPM machines have higher torque densities. As a result, FSPM machines, including fault-tolerant FSPM machines, hybrid excited FSPM machines, partitioned stator FSPM machines, and optimization strategies for FSPM machines, have been thoroughly studied. The overall performance of FSPM machines still needs to be enhanced, despite the fact that a lot of work has been done on them. In particular, FSPM machines' limited flux weakening capability needs to be improved because it seriously compromises its wide range of applications. In particular, by reducing the PM length of the standard FSPM machine and placing field windings in the spare space, "PM-top", "PM-middle", and "PM-bottom" hybrid excited FSPM machines have been analyzed. However, such machines will have limited flux regulation capability and excessive use of rare-earth PM. A switched flux memory machine with HCF and LCF PMs was created in order to address this issue. Consequently, it can enhance the ability to regulate flux while lowering the volume of rare-earth PM. However, the rare-earth PM volume is still quite significant, and the flux regulation range still needs to be expanded. An alternative flux switching memory machine with fault-tolerant features has been considered to improve the situation. Without rare earth PM, the suggested flux switching memory machine can achieve better flux regulation capabilities. The modular U-shaped stator cores are separated by the LCF PMs. The LCF magnets are wound around the DC coils that produce the magnetization current pulse. By adjusting the magnetization level of LCF PMs using a current pulse supplied by the magnetization coils, the flux linkage can be conveniently controlled. On the stator teeth, concentrated armature windings are wound in a single layer that does not overlap. There is little chance of demagnetization from the armature reaction because the magnetic flux between the LCF PMs and the reaction is parallel. The suggested FSMM's working principle is illustrated in Fig. 3.38 by means of a magnetic circuit flux path at four distinct locations that together make up a complete periodic variation of the coil flux linkage. The coil flux linkage fluctuates periodically as a result of the stator and rotor poles' alignment and misalignment. Even order harmonics are present in each coil's bipolar flux linkage, which is unexpected. However, after winding, the even order harmonics in two coils of the same phase cancel each other out, resulting in a sinusoidal flux linkage.

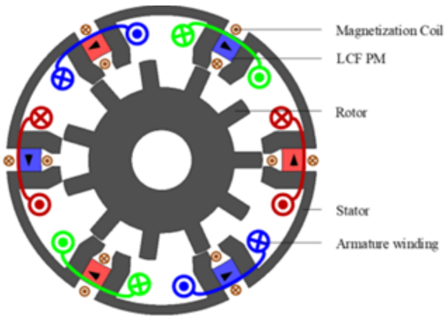

Figura 3.37: Topology of the analyzed FSMM machine.
Source: [23]

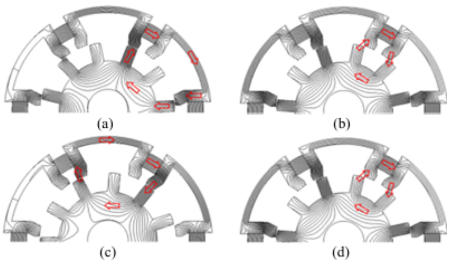

Figura 3.38: : Magnetic flux path of the analyzed FSMM at different rotor positions (a) 1st d-axis. (b) 1st q-axis. (c) 2nd d-axis. (d) 2nd q-axis.
Source: [23]

A major hysteresis loop and multiple recoil lines with varying remanent flux densities (B_{r2k}) but the same coercive force (H_{c2}) are observed in the LCF PMs. A fitted equation involving the vacuum and relative permeabilities (μ_0 and μ_r), as well as the associated re-magnetizing field (H_m) and remanent flux density (B_{rm}), can be used to express these recoil curves. The intersection of the chosen recoil line and the load line determine each magnet's operating point. It is possible to flexibly adjust the magnetization level of the LCF PMs and, in turn, the air-gap flux by changing the magnetization ratio k_m. The machine's magnetic flux distributions vary with different magnetization ratios (0%, 25%, and 100%), indicating that the FSMM's flux regulation mechanism is controllable. The stator slot number needs to be even and a multiple of the phase number (m), just like in standard FSPM machines. To guarantee balanced flux and sinusoidal back-EMF in a three-phase FSMM, the N_s and N_r combination must meet certain harmonic requirements. Analytical derivation of the armature winding's distribution factor

(k_d) and pitch factor (k_p) reveals that the maximum winding factor (k_w) happens when $N_r \approx n\, N_s \pm 1$ (where n is a positive integer). A 6-slot stator configuration is selected because the stator slots in FSMMs need to be big enough to contain the armature and magnetization windings. An 11-pole rotor is chosen as the best option in order to achieve a smooth back-EMF waveform and minimal torque ripple. The same electromagnetic principles that govern the torque and EMF characteristics of Flux Switching Permanent Magnet (FSPM) machines also govern the FSMM. The machine's back-EMF and electromagnetic torque are calculated as functions of geometrical and electromagnetic parameters, such as air-gap flux density, winding turns per phase, machine speed, and other design coefficients. The coil flux linkage and back-EMF are sinusoidal. A torque density expression is developed from these relations, illustrating the relationship between torque and the split ratio, air-gap flux, rotor pole number, and stator outer diameter:

$$T \;=\; \frac{\sqrt{2}\,\pi^2}{4}\,\frac{P_r}{P_s}\,K_s\,K_l\,K_s\,l_a\,K_{sio}^2\,A_s\,B\,D_s\,o^2\,\alpha_s\,\eta \tag{3.31}$$

Where P_r is the rotor pole number, K_l is a leakage factor, K_s is the rotor skewing factor, B is the air-gap flux, l_a is the stack length, respectively, P_s is the stator tooth number, α_s is the stator tooth arc factor, η is the machine efficiency, K_{sio} is the split ratio which can be expressed as:

$$K_{sio} = \frac{D_{si}}{D_{so}} \tag{3.32}$$

(D_{si} and D_{so} are the stator inner diameter and stator outer diameter). According to the final sizing equation, the FSMM's torque capability depends on the design parameters controlling mechanical dimensions, efficiency, and magnetic loading and scales with the square of the stator diameter. Under the same design and operating conditions, a performance comparison between the reported Flux Switching Memory Machine (FSMM) and a conventional Hybrid-Excited FSPM (HE-FSPM) was conducted. The FSMM achieves higher magnetic performance and a wider flux regulation range (0-20 V back-EMF), according to the results. Additionally, under zero magnetization of the low-coercive-force magnets, it can totally eliminate PM flux, offering exceptional fault tolerance and avoiding uncontrolled generator faults (UGF), which is a significant benefit for high-speed and low DC-voltage applications like electric drives. It can be discovered that the output torque can be freely chosen based on the various magnetization states of the LCF PMs, confirming the previously mentioned superior flux regulation capability. With regard to the torque performance of the conventional HE-FSPM under both positive and negative excitation, due to the limited ability to regulate flux, it is discovered that the output torque range is quite narrow. The output torque of this FSMM is 18.8% higher than that of its counterpart, in addition to having a large flux regulation range. it is detected that when the current angle is approximately zero for both machines, the average torque reaches its maximum value, indicating that there is no saliency and that the control of $i_d = 0$ is suitable for both machines. The risk of on-load demagnetization caused by the armature's reaction to the LCF PMs' operating points has been studied. Despite the parallel pattern of the magnetic circuit between the armature fields and LCF PMs, the cross-coupling effect between the two types of fields may result in demagnetization under on-load conditions. It is evident that the LCF PM operating points' variations are consistently higher than the knee point. Consequently, the considered FSMM has superior demagnetization resistance. For the considered FSMM, the iron loss shows an increasing trend as the magnetization level of LCF PMs increases, and the HEFSPM machine shows a similar trend. The overall iron loss of the two machines is comparable. In the analyzed FSMM, the rotor iron loss dominates the total iron loss at high magnetization levels, while the stator iron loss dominates the total iron loss at low magnetization ratios. The stator iron loss consistently accounts for the majority of the overall iron loss for the HE-FSPM. The suggested FSMM is shown to have a very wide flux regulation range and a desirable high efficiency. The FSMM outperforms its HE-FSPM counterpart in terms of efficiency and flux controllability. In short, in addition to eliminating rare earth magnets, thereby reducing costs and dependence on critical materials, and significantly expanding flux regulation, this machine offers superior torque performance and guarantees high efficiency and fault resistance (UGF tolerance). It is therefore more suitable than conventional HE-FSPM machines for electric traction applications with a wide range of speeds.

3.6 Variable Magnetization Pattern Machines

For surface permanent magnet synchronous machines (SPMSM), magnetization pattern shaping is essential because it has a direct impact on the spatial distribution of magnetic flux density in the airgap. In order to reduce losses and torque ripple, fixed forms of permanent magnet magnetization spatial distribution have been extensively studied over the decades. The most straightforward approach among these methods for designing the magnetization spatial distribution is magnet geometric shaping. This method involves cutting magnets into the desired shape during production, after which they are affixed to the machine core's surface. As an alternative, the necessary magnetization shape on the rotor core can be produced by using multiple segmented magnets. In this case, it is possible to alter the magnetization pattern by altering each magnet segment's alignment. An additional method is to form the design when the magnetic material is magnetized through a strong magnetic field, which causes the alignment of the magnetic dipole moments. The magnetization pattern in this technique is shaped by the magnetizing fixture's design. It has been investigated to use the machine core in place of a magnetizing fixture. The inability to alter the magnetization pattern after the machine is constructed is a disadvantage of these traditional magnetization shaping techniques. Another strategy for reducing torque ripple and loss is the dynamic current waveform change. For example, a method that employs sinusoidal current in the high-speed region where iron losses are more significant and square wave current in the low-speed region where switching loss predominates has been documented in the literature. To raise the fundamental voltage and expand the flux-weakening region, they suggest using square wave current in the high-speed region. In order to lower losses and enhance torque quality, variable magnetization pattern machines (VMPMs) have been introduced, because they can dynamically alter the back EMF waveform. During operation, this machine can alter the back-EMF waveform through controlled spatial demagnetization. Variable flux permanent magnet machines (VMPMs) are a subset of VFPMs. But unlike VFPMs, which only concentrate on changing the magnetization magnitude in the permanent magnets, VMPMs have an extra dynamic degree of freedom when it comes to manipulating the magnetization since they can alter both the pattern shape and the magnitude. Fig. 3.39 displays the conceptual operational image of this kind of machine. By changing the magnitude and angle of the magnetizing current vector through the stator windings, a desired magnetization pattern and, consequently, a specific back-EMF can be achieved.

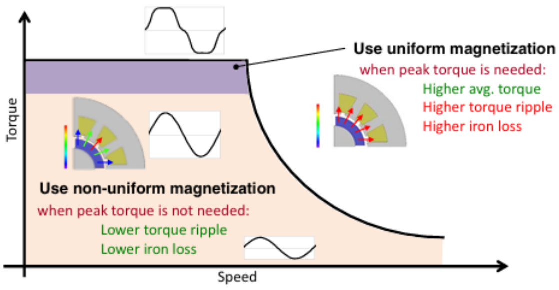

Figura 3.39: Conceptual extended N-T curve by variable magnetization pattern machine.
Source: [2]

By positioning the operating point of each permanent magnet component at the specific spot on the B-H curve that corresponds to the desired magnetization pattern, an arbitrary magnetization pattern can be achieved. The external magnetic field provided by the armature winding current regulates the position of the operating points. This kind of machine actively uses both a d-axis and a q-axis current to regulate the magnetization's spatial distribution. The magnet's edges will become demagnetized if the operating point is pushed below the knee point by a strong enough magnetic field. The benefits of VMPMs include:

- Loss reduction: By adjusting the magnetization pattern to operating conditions, VMPMs can maximize motor performance. For instance, the sinusoidal pattern is recommended for low-to-medium torque and medium-to-high speed operation because it reduces iron and copper losses, whereas the square back-EMF pattern is best suited for high-torque, low-to-medium speed operation.

- Better torque quality: By efficiently controlling the magnetization's spatial characteristics, undesirable characteristics like torque ripple and iron losses brought on by the magnetic flux density's spatial harmonic components are decreased. For instance, when compared to a uniform pattern, a sinusoidal magnetization pattern can greatly reduce torque ripple.

3.7 Variable-Magnetization IPM (VM-IPM) Motors

With PMs that can change the magnetization state with a tiny magnetizing current, an alternative IPM motor (VM-IPM motor) with high efficiency over an ample speed range is analyzed. Composite PMs and series and parallel magnetic circuits make up the suggested VM-IPM motor. We talked about the VM-IPM motor's operating characteristics over a wide speed range as well as the de-and-re-magnetization of PMs. The analysis results verify that the VM-IPM motor achieves a small magnetizing current and a wide flux range. This allows the motor to operate at high efficiency over a wide speed range and produce high torque at low speeds and an almost constant maximum power from medium to high speeds. A large coil is needed to create a high field in order to magnetize the NdFeB magnet because its coercive force is a high field of 1000 kA/m. Consequently, under the field produced by the PM motor's armature current, the NdFeB magnet's magnetic force remains constant. In traditional motors, the magnetic field generated by the armature windings is approximately 1/10 to 1/20 that obtained with large magnetizing coils. If permanent magnets have too low a coercive force (≈ 50 kA/m), they can undergo irreversible demagnetization due to the field induced by the load current, thus reducing the motor's torque. For this reason, magnets intended for flux regulation must have a coercivity between 100 and 300 kA/m. Low-coercivity SmCo magnets, called VPM (Variable Permanent Magnets), are used for this purpose. The considered VM-IPM motor is a variant of the IPM (Interior Permanent Magnet) type, capable of regulating the magnetic flux by applying a current along the d-axis:

- a positive current along the d-axis re-magnetizes the magnet,
- a negative current along the d-axis demagnetizes it.

However, it is difficult to reconcile a low magnetizing current (typical of series configurations) with a wide back-EMF adjustment range (resulting from parallel configurations). Despite this, VM-IPM motors can generate high torque at low speeds and constant power at medium and high speeds. The design goal is to keep the magnetizing current less than twice the rated inverter current, thus ensuring high efficiency and magnetic stability. The considered motor rotor has a salient core with two “V”-shaped flux barriers (inner and outer), each containing pairs of permanent magnets, VPM and CPM, arranged to form magnetic circuits both in series and in parallel. The VPM can vary its magnetization state from negative, to zero, to a maximum positive value, producing a wide range of controllable flux and back-EMF. The series connection between VPM and CPM allows to significantly reduce the current required for re-magnetization, since the field generated by the CPM adds to that produced by the magnetizing current, facilitating the variation of the magnetic state of the VPM. The double V-shaped flux barrier configuration also helps increase reluctance torque, thanks to the large reluctance difference between the d and q axes. Furthermore, the diagonal series connection of the two CPMs allows for high magnetic flux density to be maintained without penalizing re-magnetization, thus increasing overall torque and power. To further improve the re-magnetization of the internal magnet, a composite magnet was introduced, consisting of a VPM layer superimposed on a CPM layer. The CPM field assists the VPM field, allowing re-magnetization with low currents. Two variants have been considered:

1. Composite with C-PM in parallel, which facilitates magnetization in difficult areas.
2. Composite with C-PM in series, where the C-PM layer strengthens the V-PM magnetic field, increasing power and magnetic stability.

In the final configuration, the VPMs and CPMs are alternated in the two "V" flux barriers. This architecture combines the advantages of series and parallel connections, allowing the motor to achieve: a wide range of magnetic flux regulation, low magnetizing currents, high torque density, and constant power over a wide speed range. To verify the feasibility and magnetic behavior of the VM-IPM (Variable Magnetization Interior Permanent Magnet) motor, a magnetic field analysis was conducted using the finite element method (FEM) using J-MAG software. The objective was to study the demagnetization and re-magnetization processes of low-coercivity magnets (VPM) and the resulting variation in the generated back EMF. The results indicate that, after demagnetization, the total magnetic flux is reduced to approximately 66.6% and 65.0% of the maximum value for the parallel and series CPM configurations, respectively. After re-magnetization, the flux returns to approximately 94.3% and 93.4% of the original maximum value. These results confirm that the analyzed VM-IPM motor is capable of effectively regulating the magnetic flux using magnetizing currents approximately twice the nominal current, enabling reversible and stable flux regulation without significant performance loss. Using magnetic FEM analyses, the electromagnetic torque was calculated for different current phases at a nominal current of 180 A_{rms}. The results show that the maximum torque is achieved for a current phase of approximately 131°-132°, for the motor versions with composite magnets containing CPMs in parallel and in series, respectively. The phase advance with respect to the q-axis (90°) highlights that the V-shaped flux barriers effectively contribute to the reluctance torque, increasing the total available torque. The dynamic performance of the motor in terms of torque, power and voltage was evaluated over a wide speed range (0-30,000 rpm), considering three magnetization states of the V-PMs: full magnetization, demagnetization and re-magnetization. Both VM-IPM motors maintain a constant power output above 50 kW from 6,000 to 30,000 rpm, demonstrating excellent magnetic flux and torque adapting capabilities across the entire operating range. Efficiency and loss maps show that VM-IPM motors operate at high efficiency up to 10,000 rpm, but efficiency decreases at higher speeds due to reduced output power and increased copper and iron losses. Permanent magnet losses are highest in the fully magnetized and re-magnetized states, while the demagnetized state offers lower iron and copper losses due to the reduction in total magnetic flux and field weakening current. As a result, the motor exhibits higher efficiency at high speeds when operating in a demagnetized state.

3.7.1 Experimental Validation

As a benchmark for the Nissan LEAF traction drive, Yoneda, Suzuki, and Sakai (2022) developed and experimentally validated a 100 kW Variable-Magnetization Interior Permanent-Magnet (VM-IPM) motor, building on the variable-magnetization principle first put forth by Sakai et al. (2021). The study's objective was to validate the VM-IPM concept's viability and efficiency benefits in a comprehensive automotive application. Two types of permanent magnets are embedded in the dual V-shaped rotor of the suggested machine: a CPM made of high-coercivity NdFeB and a VPM made of low-coercivity SmCo. By applying tiny magnetizing currents along the d-axis, these magnets can be magnetically coupled via a hybrid series–parallel magnetic circuit, enabling both flux-enhancement and flux-weakening operations. A magnetizing current of ±2 p.u. (double the rated current) is adequate to achieve a significant flux variation without the risk of irreversible demagnetization, according to experimental tests and finite-element analysis (FEA). It was demonstrated that the back-EMF amplitude varied between fully demagnetized and fully magnetized states, ranging from 65.4% to 93.9%. The performance of the VM-IPM was nearly identical to that of the original Nissan LEAF motor under these circumstances, with a maximum torque of 332.5 N · m and a peak power output of 96 kW. Reduced copper and iron losses at partial magnetization levels were responsible for the suggested motor's average efficiency improvement of +2.8 to +4.6 percent in the high-speed and extra-high-speed regions when tested under WLTC driving cycles. The dual-V hybrid-magnetic design, according to the authors, provides a workable way to integrate variable-magnetization technology in commercial EV traction systems by allowing wide flux control with low excitation current. Thus, the VM-IPM concept sets another standard for high-efficiency, wide-speed-range electric drives by proving both theoretical viability and industrial applicability.

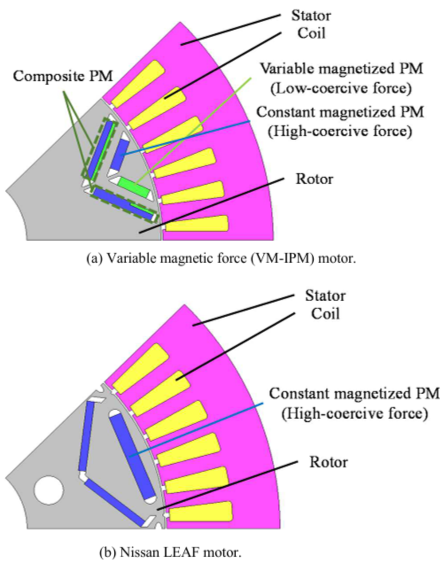

Figura 3.40: Configurations of the VM-IPM and Nissan LEAF motors.
Source: [13]

3.8 Other examined architectures

3.8.1 Axial-field Juxtaposed Magnetic Circuit VFMM

An axial juxtaposed magnetic circuit variable flux memory machine (AF-JMCVFMM) is taken into consideration to achieve a wide speed control range and high efficiency at high speeds. The goal is to combine the high power density of axial juxtaposed magnetic circuit variable flux memory machines (AFPMMs) with the flux control capabilities of VFMMs, making them suitable for variable-speed traction applications such as electric vehicles. It has an axial structure (AFPMM) with a stator made of SMC material to provide a 3D magnetic circuit and reduce iron losses at high speeds. PMs placed on a double layer (inner and outer):

- LCF PM to provide the adjustable magnetic field.
- HCF PM to provide the stable field.

It features two rotor topologies:

1. AF-JMCVFMM1: HCF PM with conventional N-S poles, symmetrical fluxes, and lower torque ripple.
2. AF-JMCVFMM2: HCF PM with consequent-pole on the outer layer, with a wider flux adjustment range and lower consumption of rare earths, but higher torque ripple.

In the flux-enhanced state, the LCF PM is magnetized in the same direction as the HCF PM, resulting in an increase in the magnetic flux in the air gap. In the flux-weakened state, however, the LCF PM is magnetized in the opposite direction, resulting in a reduction in the magnetic flux in the air gap and an expansion of the speed range. The uncoupled juxtaposed topology of the AF-JMCVFMM1 improves resistance to accidental demagnetization compared to conventional PMCT-VFMMs. At no load, both machines exhibit excellent flux regulation capabilities. The AF-JMCVFMM1 has a more sinusoidal back-EMF, while the AF-JMCVFMM2 requires smaller current pulses for magnetization/demagnetization. At load, the AF-JMCVFMM1 exhibits higher torque density and low ripple. On the other hand, the AF-JMCVFMM2 exhibits higher torque ripple but better speed expansion and less use of rare earth PM. Regarding efficiency, both machines exhibit high efficiency, with the high-efficiency zone extending to high speeds.

3.8.2 Dual-Sided VFMM

A dual-sided permanent magnet memory machine (DSPM-MM) has been analyzed that combines the high torque density typical of PM machines on the rotor with the easy magnetic flux control typical of PM LCF memory machines on the stator, reducing copper flux weakening losses. The rotor has permanent NdFeB magnets with consecutive poles alternating with iron poles, while on the stator we find low coercive force magnets (AlNiCo) inserted between the stator teeth, wrapped by direct current magnetization coils, as shown in Fig. 3.41. There is a double flux modulation effect: both the PMs on the stator and those on the rotor contribute to and modulate each other. This increases torque and improves efficiency. An

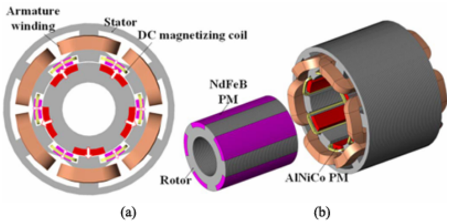

Figura 3.41: Examined DSPM-MM. (a) Configuration. (b) Cross-sectional view. Source: [22]

analysis was performed on 4-, 5-, 7- and 8-pole rotor configurations. It emerged that the greater the number of rotor poles, the greater the flux regulation range. Furthermore, machines with an even number of poles exhibit higher average torque but also more torque ripple. However, iron losses increase with more poles but can be reduced by adjusting the MS of the PM LCFs. The six-PM-stators/seven-PM-rotors configuration proved to be the most balanced in terms of torque, efficiency and adjustment range, and was chosen to build a prototype.

3.8.3 Wide Speed-Regulated Reverse Salient-Pole Variable Leakage Flux IPM Machine

An alternative internal permanent magnet (IPM) synchronous motor called RSP-VLF-IPM was analyzed, designed to achieve wider speed regulation, better high-speed efficiency, and lower risk of demagnetization compared to traditional IPM motors. The aim is to control leakage flux through the armature's magnetomotive force, combining two features: RSP (Reverse Salient-Pole), which increases the d-axis inductance ($L_d > L_q$), useful for extending the speed range, and VLF (Variable Leakage Flux), which allows the magnetic flux to be varied by adjusting the q-axis current, improving the regulation of the magnetic field in the air gap. This motor features NdFeB PMs arranged internally in the rotor. The stator consists of 48 slots and 8 poles, with a single-layer distributed winding and a star (Y) connection. The rotor features an advanced topology compared to a traditional IPM, with: adjustable leakage flux paths, magnetic barriers along the q-axis to achieve L_d $> L_q$, multilevel ladder-shaped magnetic barriers and two arc barriers to reduce torque fluctuations and improve robustness, and magnetic bridges inserted into the permanent magnets to increase mechanical strength. In the VLF topology, the q-axis current controls the leakage flux between the magnetic poles: therefore, with low q-current, more flux is obtained in the air gap (a stronger magnet), while with high q-current, more leakage flux is obtained (a “weakened” magnet). In RSP topology, however, the motor operates in a region of field enhancement with positive d-axis current ($i_d > 0$), reducing the risk of demagnetization and increasing useful torque at high speeds. There is a noticeable change in inductance with current in the RSP-VLF-IPM motor. When id is positive, a positive reluctance torque results from L_q sharply decreasing as the q-axis current increases while L_d stays higher. The flux-weakening performance is improved by this behavior. The RSP-VLF-IPM motor channels a portion of the armature flux through the low-reluctance leakage path, in contrast to the conventional IPM motor, where the d-axis flux linkage decreases as a result of armature reaction. By enabling controlled flux variation of up to 24%, this mechanism enhances adaptability to changes in load. The RSP-VLF-IPM motor operates in the magnetic field enhancement region ($L_d > L_q$), achieving its maximum torque at a positive i_d with a lower demagnetization risk, despite producing a slightly lower peak torque. Its design significantly minimizes cogging torque and torque ripple, resulting in less noise and more smooth operation. Compared to the conventional IPM, which operates at less than 5000 rpm, the RSP-VLF-IPM motor achieves a greater constant-power speed range, reaching 6000 rpm. At higher speeds, its output power stays constant, indicating better power density and flux-weakening ability. Due to less magnetic saturation, the RSP-VLF-IPM motor has lower iron and copper losses, especially in the constant-torque region, according to finite element analysis. At medium and high speeds, its efficiency outperforms that of the traditional IPM by 1-4%, which makes it more appropriate for variable-speed drive applications like electric cars.

3.8.4 Iron-Nitride-Based PM VFM

The application of iron nitride (FeN) magnetic material in variable flux motors (VFM) was evaluated to: reduce the use of rare-earth magnets, maintain high electromagnetic performance (torque, flux, efficiency), expand the flux control range and operating speed range, and avoid the risk of irreversible demagnetization typical of rare-earth magnets. Two types of reference machines and their modified versions with FeN magnets were analyzed: variable-flux inverted reluctance motor and series hybrid variable-flux motor. The FeN magnet, having high residual flux density and high coercivity, allows to maintain good performance with less volume of magnetic material, but requires higher currents for re-magnetization. A two-line hysteresis loop (BH) approximation model is used to characterize FeN and AlNiCo magnets. The main parameters considered are residual flux density (B_r), coercivity (H_c), differential permeability, and slope of the demagnetization curves. It is shown that the FeN magnet has a 25% higher Br and a 166% higher Hc than the AlNiCo9. For the inverted reluctance motor, for the same magnet volume, FeN increases: air gap flux density by +34.5%; back-EMF by +33%; and average torque by +22%. After optimization, the use of the FeN magnet allows for a 46% reduction in PM volume and rotor weight. However, the required re-magnetization current is approximately 60% higher than that of AlNiCo9. For the series hybrid motor (FeN + AlNiCo), two combinations were tested: FeN-AlNiCo9 and FeN-AlNiCo5. Both completely eliminate the use of rare earth elements, maintaining a constant torque similar to the original NdFeB motor. The FeN-AlNiCo9 combination exhibits a better resistance to demagnetization under load (only a 10% reduction in flux) and a re-magnetization current approximately 4 times the nominal (acceptable in modern EV applications). The operating speed range extends up to 5400 rpm, maintaining good efficiency at moderate magnetization. At low speeds, maximum magnetization is preferable (maximum torque and efficiency), while at high speeds, reduced magnetization is preferable (lower losses and a wider constant power range). Efficiency improves during high-speed operation, with a smoother transition between the constant torque and constant power regions.

3.8.5 Hybrid-Excited Flux-Modulated Memory Machine for Electrical CVT System

An hybrid excitation double-rotor, double-stator machine (HEFMM - Hybrid Excitation Flux-Modulated Memory Machine) has also been analyzed, aiming to integrate the E-CVT (electric continuously variable transmission) system into HEVs to improve torque density, efficiency and speed range. The machine consists of two rotors and two stators. The internal MFMMM (Memory Flux-Modulated Machine) serves as the primary motor, connected directly to the transmission line. The external DVPM (Dual Variable-flux Permanent Magnet Machine) serves as an auxiliary motor, connected to the internal combustion engine (ICE). AlNiCo permanent magnets (LCF) allow flux regulation via DC current pulses. In hill climb or start mode, the ICE kicks in, activating the auxiliary motor to provide more power. In regenerative braking mode, kinetic energy is converted into electrical energy and stored in the battery/ultracapacitor. The DC pulse in the magnetization windings regulates the level of back-EMF, and by reducing it, increases the speed range and thus improves efficiency. In climbing or starting up mode, the ICE kicks in, activating the auxiliary motor to provide more power. In regenerative braking mode, kinetic energy is converted into electrical energy and stored in the battery/ultracapacitor. The DC pulse in the magnetization windings regulates the level of back-EMF, and by reducing it, increases the speed range and thus improves efficiency. A simple flux control is achieved just by reversing the direction of the DC pulse. The back-EMF of the internal winding is adjustable (from 50 V to 30 V after demagnetization). The external winding remains stable during magnetization/demagnetization. The torque of the internal rotor is adjustable, and the E-CVT system achieves greater efficiency over a wide speed range.

VFMM with Self-Flux Leakage Path

This other variable flux memory machine with a self-flux leakage path can expand the magnetic flux adjustment range, maintain high torque density and reduce the required magnetizing current. An equal number of HCF PMs are positioned in spoke-like configurations between the neighbouring LCF PMs, while the utilized LCF PMs are positioned circumferentially close to the airgap. At both ends of the LCF PMs are a few short HCF PMs. At the end of the spoke HCF PMs, which are only functional in the demagnetization state, some self-flux leakage pathways are built. By using transient magnetization or demagnetization current pulses, the spoke HCF PMs can stabilize the MSs of the LCF PMs and modify them. In the case of positive MS (magnetization), the flux generated by the HCF PMs is forced to pass through the LCFs by the armature current, resulting in high flux density in the air gap and no leakage. In the case of negative MS (demagnetization), the LCF PMs are demagnetized and short-circuited, causing the flux to leak through the leakage paths and consequently greatly reducing the flux density in the air gap. The advantages of this configuration are:

- Reduced magnetizing current required, thus reducing inverter power requirements.
- Greater flux regulation range, thus achieving a wider speed range.
- High torque density is maintained, useful for electric vehicles and high-performance applications.

3.9 Scalability and Key Tradeoffs of VFPMM

For an extensive range of power specifications, the scalability of important VF-PMSM performance metrics, including torque, power capability, and MS variation limits, as well as their effects on driving cycle losses and system cost, have been investigated. The VF-PMSM considered has a topology that consists of a series combination of low-H_c magnets (SmCo) and high-H_c magnets (NdFeB) placed in a rotor with large q-axis flux barriers to help in the magnetization process and guard against demagnetization due to load current. The stator is made up of hairpin windings to increase the slot fill factor and distributed windings with 2.5 slots per pole per phase to produce a distribution of magnetomotive force (MMF) that is almost sinusoidal. The thickness weighted average of the magnetization (J) of the two types of magnets is known as the equivalent magnetization (J_e). The ratio of the current magnetization (J_e) to the maximum achievable magnetization (J_{e-max}) is known as the magnetization state (MS). Key parameters like J_{e-max} and J_{e-min}, which can be reached within the inverter's current limit, as well as the permanent magnet flux linkage (λ_{pm}), inductances (L_d, L_q), and the demagnetization boundary, must first be estimated in order to determine the performance capability of VF-PMSMs. (J_{e-max} - J_{e-min})/J_{e-max} x 100 [%] is the definition of the MS variation range. In a simplified d-axis magnetic circuit model (MCM) of a single pole, the effective reluctances are determined using the flux paths induced by the magnet MMF and those induced by the stator MMF excited by i_d current (taking into account symmetry of the fundamental model). J_{e-max}, J_{e-min},λ_{pm}, and Ld are estimated using this d-axis MCM in conjunction with the J-H properties of the magnet material. To estimate L_q, a comparable circuit that captures the q-axis flux paths is created. The peak torque capability is estimated by applying the peak current and changing the current angle (β) from -90 to 90 degrees. The maximum demagnetizing MMF observed by the magnets is estimated for each current angle. To determine whether it can induce demagnetization, this MMF is used to excite the d-axis MCM. For current angles that do not result in demagnetization, torque is computed using (λ_{pm}, L_d, L_q). The upper bound for the peak power in conventional PMSMs is defined by the characteristic current ($i_{d0} = \lambda_{pm}/L_d$), normalized by the rated current. The magnet in VF-PMSMs may become demagnetized by -i_d current, which would cause λ_{pm} to decrease as Id increases. Therefore, it is necessary to estimate the effective i_{d0} while taking the demagnetization behaviour into account. The MS and λ_d change as Fig. 3.42a illustrates, beginning with an initial magnetization of Je-max and applying increasing magnitudes of -i_d. As applied to an example VF-PMSM at 100% MS and 75% MS, respectively, Figures 3.42b and 3.42c show the variations in i_{dq} operating points along the torque-speed envelope computed using techniques outlined in for conventional machines. The demagnetization boundary limits the maximum torque per volt (MTPV) curve for conventional PMSMs (B_i-C_i) to (B-C). As shown in Figs. 3.42b and 3.42c, the demagnetization boundary moves to the left, and the point C_i moves to the right as MS drops from 100% to 75%. Therefore, it is feasible to operate at the corresponding C_i (i.e., the Id0 for that MS) at medium/low MS; however, the current magnitude decreases with MS. Therefore, at an intermediate MS, where the demagnetization boundary meets C, the feasible i_{d0} is maximized. Thus, the d-axis MCM and the λ_d vs. -i_d curve can be used to estimate the maximum power at high speed for VF-PMSMs. All geometric dimensions are scaled proportionally to the stator's outer radius (R_{so}), keeping the current density constant (22.1 A_{rms}/mm^2). The magnet retaining bridles are resized to withstand centrifugal stresses up to 10,000 rpm. The results obtained through analytical modeling and FEM simulations show good agreement. Scaling leads to an increase in the stator magnetomotive force (MMF) proportional to R_{so^2}, greater than the increase in the magnet MMF, which increases linearly with R_{so}. This results in greater ease of magnetization and demagnetization, as well as an increase in inductance. However, although torque increases approximately with $R_{so}^{2.83}$, normalized power at high speed tends

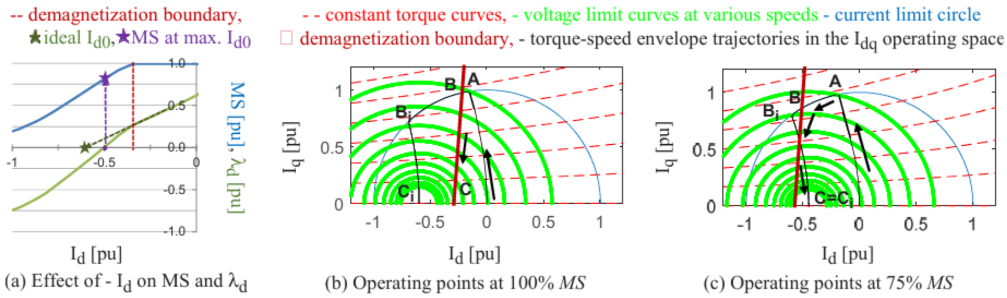

Figura 3.42: Variation of characteristic current, MTPV curve in VF-PMSMs with MS change.
Source: [3]

to decrease due to the greater susceptibility to demagnetization and the increase in inductance.Three crucial geometric factors are determined in order to alleviate these effects: the ratio of stator internal to external radius (R_{si}/R_{so}), the ratio of high-coercivity magnet thickness to total magnet thickness (m_{th}/m_t), and the ratio of magnet thickness to stator internal radius (m_t/R_{si}).

- m_t/R_{si}: A value that is too high restricts excitation current and lowers power; a value that is too low encourages flux variation and lowers flux losses in the rotor but may result in demagnetization. There must be a compromise.
- m_{th}/m_t: Lowering this ratio increases the range of magnetic regulation, but it also decreases maximum power and ease of magnetization.
- R_{si}/R_{so}: Lowering this ratio improves the stator/magnetic MMF ratio and flux regulation capability; however, high values result in demagnetization and increased inductance. When the MMF ratio is close to 1, the ideal result is achieved.

The reference design includes over 11 geometric variables, subject to electromagnetic, mechanical, and thermal constraints, such as iron saturation, maximum current density, and centrifugal stresses on the magnets at 10,000 rpm. These constraints reduce the number of independent parameters to four: magnet thickness (m_t), stator core length (s_l), stator outer radius (R_{so}), and rated current (i_R). Once these parameters are fixed, the high-coercivity magnet thickness (m_{th}) and optimal axial length are determined to meet the required power and torque. The following conclusions are drawn:

- VF-PMSM designs have a greater torque capability and a higher MS manipulation range when scaled proportionately to the stator outer radius, but a lower high-speed power capability normalized by the inverter capacity.

- The demagnetization characteristics determine whether it is feasible to operate at the current, and the characteristic current for VF-PMSMs varies with the MS. The maximum characteristic current that can be achieved within the demagnetization limits determines the maximum normalized power capability of VF-PMSMs.
- Oversizing the inverter capacity may be necessary to increase the VF-PMSM's power capability; however, the variable MS's ability to reduce loss can lower the battery capacity needed to reach a desired driving range.
- As the MS variation range rises to about 50%, the cost of battery capacity can be significantly reduced, effectively offsetting the cost of increased inverter current capacity.
- VF PMSMs can reduce driving cycle loss over a large range of peak power ratings. Using design examples from 120 kW to 275 kW rating machines, it has been demonstrated that variable MS control reduces loss by 14-28% over a range of standard driving cycles when compared to a fixed MS operation.

3.10 Various magnet arrangements

Variable Flux Memory Machines (VFMMs) and associated variable-magnetization motors have been considered with a wide range of permanent magnet configurations in recent years. By altering the magnetic circuit topology or the magnets' spatial arrangement, each configuration wants to produce particular electromagnetic benefits. Parallel and hybrid magnetic circuits increase the flux-regulation range, while series-type structures increase the demagnetization withstand capability. Furthermore, a certain number of rotor and stator geometries have been studied in order to maximize air-gap flux distribution, torque density, and efficiency. These include U-shaped, V-shaped, delta-type, dual-layer, and split-spoke configurations. These various magnetic configurations demonstrate the continuous research attempt of achieving a balance between robustness under changing load and speed conditions, high torque output, and wide flux controllability. As regards hybrid magnetic circuit motors (HMC-VFMM), the following configuration has been examined: A spoke-type branch placed in series contributes to demagnetization resistance, while a U-shaped PM branch serves as the parallel path offering vast flux regulation. The hybrid circuit achieves a balance between on-load robustness and flux-adjustment capability. The HMC-VFMM successfully addresses the trade-offs of the classical topologies by varying the air-gap flux widely while retaining magnetic stability, as demonstrated by experimental prototypes. Bidirectional magnetization of AlNiCo magnets is made easier by the U-shaped magnet arrangement, which is commonly used in switched-flux or hybrid circuits. It concentrates magnetic flux around the stator teeth. Its structural simplicity makes it appropriate for Switched-Flux Memory Machines (SFMMs) by enabling efficient coupling between magnetization coils and PMs. Compact design and simplicity of magnetization control are advantages, but if improperly optimized, torque ripple and increased leakage flux are drawbacks. The considered Variable Magnetization IPM (VM-IPM) designs adopted the V-shaped configuration, which is typical of Interior Permanent Magnet (IPM) motors. This configuration embeds low-coercivity PMs (VPMs) and high-coercivity PMs (CPMs) in two V-shaped layers within the rotor. The materials' combination maintains a high torque density while enabling flux control through tiny magnetizing currents. Although manufacturing complexity and accurate control of magnetization currents are necessary, V-shaped configurations achieve high efficiency and wide constant-power operation ranges. The Fig 3.43 shows an HMC-VFMM, which is geometrically defined by an integer-slot distributed winding configuration and a 48-stator-slot/8-rotor-pole combination. In the meantime, the rotor structure has a PM arrangement of the delta type. A Dual Layer structure is created for the suggested machine by separating the parallel hybrid magnets and the assisted NdFeB PMs. In particular, the HCF "V"-shaped PMs are positioned on both sides of the LCF magnet, whereas the "flat type" LCF PMs are situated near the air gap. Meanwhile, the iron bridges are positioned in the middle of the V-shaped layer between two adjacent NdFeB magnets. The following benefits may be offered by the suggested HMC-VFMM design.

1. The HMC-type hybrid PM structure combines the advantages of on-load MS stabilization capability in the series structure and a broad MS manipulation range in the parallel structure.

2. By forming a series structure, the Dual Layer hybrid PM arrangement reduces the possibility of the LCF PMs accidentally demagnetizing.

3. By providing a path for the magnetization current to bypass, the iron bridge makes it possible to reduce the necessary inverter rating.

Split-spoke and dual-layer configurations, in which PMs are separated into several segments or stacked layers, are examples of later developments. These configurations allow for independent control of the magnetization states in each layer and enhance flux concentration. They reduce magnetic cross-coupling and leakage flux. Such designs, however, raise manufacturing costs and structural complexity, and accurate flux prediction necessitates precise hysteresis modelling.

3.11 Unipolar Leakage Flux

The VPMs' working points are inherently hard to maintain, and the CPMs have a tendency to inadvertently demagnetize them. In order to solve this issue, series

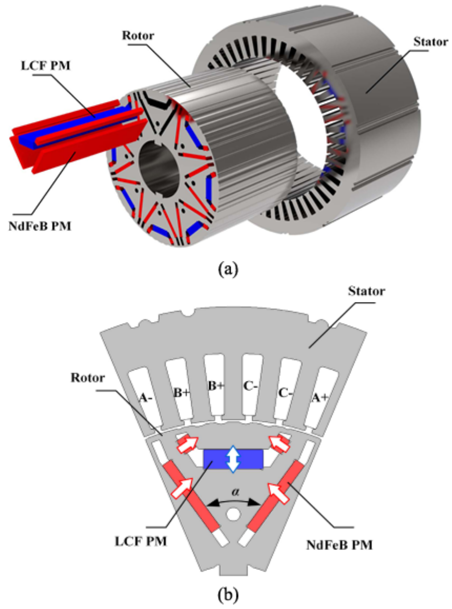

Figura 3.43: Analyzed HMC-VFMM with delta-PM configuration.
(a) 3-D view. (b) Cross section.
Source: [14]

hybrid VFM machines were developed, in which the CPMs and VPMs are positioned on the alternating poles to create a series magnetic connection. While the high armature current is appropriate because of the VPM's stable working point (due to series connection), the CPM flux would pass through the VPM and help it to resist unplanned demagnetization. As a result, the torque density is significantly increased and is comparable with standard interior-PM (IPM) machines. However, the considered VFM machine experiences magnetic unbalance, leading to unipolar z-axis leakage flux, because of the different PMs on the alternate poles. The z-axis leakage flux not only decreases torque output, but also compromise the mechanical components, such as bearing life. The 48-stator-slot/8-rotor pole configuration, which is the same as the commercial Prius 2010 IPM machine, is used. It has distributed windings to generate reluctance torque. In order to accomplish the series connection, where all VPMs have the same polarity and all CPMs have the opposite, the VPMs and CPMs are also alternately accommodated on the adjacent rotor poles. From the magnetization curves, it is observed that the VPM has a relatively low coercive force, but a higher knee point in the second quadrant of the B-H characteristic. When a high negative magnetomotive force (MMF) is applied, the VPM's operating point can drop below the knee point, causing a permanent reduction in the residual flux density (B_r) after the MMF is removed. The magnet only partially recovers along the recoil line, reaching an other residual flux density of $B_{rk} < B_r$. The open-circuit field distributions show that:

- with a fully magnetized VPM ($k_m = 100\%$), the magnetic field in the air gap is strong;
- with a demagnetized VPM ($k_m = 0\%$), the field is much weaker, while maintaining the correct polarity thanks to the CPMs.

The comparison of the back-EMF waveforms confirms that the amplitude decreases dramatically in the demagnetized state, demonstrating the system's ability to vary the magnetic flux. It is also noted that the waveforms remain symmetrical, thanks to the correct winding configuration. The cross-sectional areas of the two magnets must be inversely proportional to their remanent flux densities in order to prevent unipolar leakage flux, according to analytical modelling. Finite element analysis verifies that the leakage flux is minimized when the area ratio $A_{VPM}/A_{CPM} \approx B_{rCPM}/B_{rVPM}$. On the other hand, magnetic imbalance and saturation result in a stronger end leakage flux through the shaft if the load current increases or the VPM magnetization ratio km decreases. explains the disparity between 2D and 3D torque predictions and in addition causes unbalanced rotor poles. Therefore, stable flux regulation and the reduction of end effects depend on proper VPM-CPM design. It can be summarized that fluxes generated by CPMs and VPMs on the alternate poles may not be balanced in series hybrid VFM machines, where the unipolar end leakage flux is discovered. It is discovered that one crucial factor influencing the unipolar leakage flux is the cross-section area ratio between CPM and VPM.

3.12 Magnet Temperature Effects

The magnet magnetization J in variable-flux machines can be controlled using a variety of techniques. D-axis pulse techniques were presented, which use brief d-axis current pulses to facilitate demagnetization or magnetization while successfully removing torque ripple. However, when increasing the magnetization state, these methods show a significant low-speed limitation due to restricted inverter voltage. A reverse rotating current vector trajectory method was suggested as a solution to this problem, providing a moderate increase in speed capability. The Straight-Line Stationary Frame Trajectory ($SL\lambda^sT$), which showed a higher achievable speed and improved energy efficiency over driving cycles, was introduced after further analysis revealed the key drive properties limiting maximum speed for such trajectories. Open-loop voltage control was used to experimentally implement the $SL\lambda^sT$ for the trajectory's straight-line segments. Open-loop control, however, is susceptible to changes in parameters, especially temperature, which can have a substantial impact on magnet properties and, if left unchecked, compromise $SL\lambda^sT$ performance. It has been investigated how magnet temperature affects magnetization behavior, including the necessary current and flux vectors, maximum torque capability, and magnetization trajectories. Additionally, a compensation method is suggested to lessen the degradation brought on by temperature during $SL\lambda^sT$-based magnetization control. Finite element analysis (FEA) and experimental validation are conducted using a variable-flux (VF) test machine with a peak power rating of 80 kW. By temporarily using a current/flux linkage (i_{dq}/λ_{dq}) vector that modifies the internal magnetization J of the permanent magnets, VF machines are able to achieve a variable permanent magnet flux linkage λ_{pm}. Normal operation, such as loss minimizing current vector control, is resumed until it is desired to change J again following a brief trajectory that results in magnetization (increasing J) or demagnetization (decreasing J). Magnetization can be altered within drive current limits by using low-coercivity magnets. The required voltage may be high due to the large flux linkage during the magnetization trajectory, imposing a speed limit based on the voltage capability of the inverter. When resistance is ignored, a d-axis pulse's peak phase voltage is roughly:

$$v_{\text{phase, peak}} \approx \omega_e, \lambda_{\text{mag}} \tag{3.33}$$

and its maximum speed is:

$$\omega_{\text{max}} \approx \omega_{\text{base}} \cdot \left(\frac{\lambda_{\text{MTPA}}}{\lambda_{\text{mag}}} \right) \tag{3.34}$$

where λ_{mag} is the λ_d required to increase the preferred magnetization level, λ_{MTPA} is the total stator flux linkage at the maximum torque per amp with rated current, ω_e is the rotor speed, and ω_{base} is the base speed. Using a dynamometer equipped with thermocouples on stator coils and magnets (through a slip ring), the test platform is a salient-pole VF-PMSM (peak power 80 kW). Two types of magnets are used in the rotor: low-H_c SmCo with variable magnetization (J_{low-Hc}) and high-H_c NdFeB with fixed magnetization ($J_{high-Hc}$). A thickness-weighted average can be used to define an equivalent magnetization J_{eq} for the combined magnets:

$$J_{\text{eq}} = \frac{J_{\text{low-Hc}}.t_{\text{low-Hc}} + J_{\text{high-Hc}}.t_{\text{high-Hc}}}{t_{\text{low-Hc}} + t_{\text{high-Hc}}} \tag{3.35}$$

Where t_{low-Hc} and $t_{high-Hc}$ are the thicknesses of the two magnets. For both high and low H_c magnets, FEA of the test equipment was performed at different temperatures. In order to determine the integral average of the magnetization of the low H_c magnets, or J_{low-Hc}, which corresponds to the maximum and minimum possible J_{low-Hc} at that temperature, the full magnetization (i_d = 503 A) and full demagnetization (i_d = -503 A) conditions are first assessed using the full nonlinear temperature-dependent B-H curve of the low H_c magnet. In order to create maps of the fundamental flux linkage and magnetization in the current plane once full magnetization has taken place, the maximum J_{low-Hc} is then set as the initial magnetization condition and evaluated at different i_{dq} operating points. Similarly, maps following complete demagnetization are subjected to the minimum J_{low-Hc}. The obtained curves represent the entire magnetization capability envelope within the machine's 503 A rated current limit. Both J_{eq} and J_{low-Hc} have larger minimum values as the magnets' temperature rises, but the maximum J_{eq} hardly changes and the maximum J_{low-Hc} increases at all. The magnets are more readily demagnetized as the temperature rises because demagnetization happens with less negative id. Saturation of the curves is visible at high currents, but aside from the envelope corners, the relationship between λ_d and J_{eq} is essentially linear. The maximum torque occurs at a smaller β but similar J_{eq} as the magnet temperature rises. As β and temperature rise, J_{eq} becomes more demagnetized. Notably, the maximum torque condition has a larger stator flux linkage at 110 °C, which will result in a 4% drop in base speed. After complete magnetization and demagnetization, the λ_d versus id relationship is displayed in Fig. 3.44(a). At lower λ_d, magnet temperature only has a significant impact. Fig. 3.44(b) shows the estimated maximum speed for increasing to a desired J_{eq} when using d-axis pulse methods. The speed limit for increasing to the maximum J_{eq} is lower than the base speed, indicating that higher speed methods, like the $SL\lambda^sT$, are required to fully magnetize and achieve maximum torque above low speeds. Magnet temperature only affects the lower J_{eq} region.To evaluate the effects of magnet temperature on torque characteristics and magnetization, the VF-PMSM prototype underwent experimental testing. Near room temperature and a higher temperature achieved by heating the magnets with high-frequency id pulses were the two thermal conditions that were investigated. In order to estimate the flux linkage (λ_{pm}), which represents the equivalent magnetization J_{eq}, the machine was magnetized and demagnetized using different id pulse amplitudes. The no-load back-EMF was then measured. The findings indicated that while magnetization necessitates slightly smaller current amplitudes and yields a slightly higher λ_{pm}, demagnetization happens with a smaller negative id and a lower minimum λ_{pm} at higher magnet temperatures. Maximum torque drops under rated load and happens at a smaller current phase angle (β), confirming that high temperature promotes demagnetization, which is in line with FEA predictions. A closed-loop Straight-Line Stationary Frame Trajectory (CL-$SL\lambda^sT$) method was developed to mitigate the effect of magnet temperature on magnetization control. Even when operating at high speeds and with limited inverter voltage, the method controls transient flux-linkage trajectories that are used to alter the magnetization level (J) without going over the demagnetization boundary. The suggested closed-loop method uses flux-linkage feedback from an observer model to continuously update the trajectory and voltage commands at each PWM sampling period, in contrast to open-loop voltage feedforward implementations that are extremely sensitive to temperature and parameter changes. The flux observer estimates the dq-axis flux linkage with high accuracy by combining open-loop voltage and current models. This enables safe magnetization paths to be maintained through real-time trajectory adjustment. In order to prevent demagnetization, the system automatically splits the second half of the trajectory into two linear segments tangent to the maximum flux limit at higher temperatures, as demonstrated by simulations and experiments conducted at 30 °C and 80 °C. Experiments showed robustness against temperature changes and verified precise magnetization control with MSe errors less than 3%. Because of the short trajectory duration (less than 3 ms), the method also reduced torque ripple. Overall, CL-$SL\lambda^sT$ improves the efficiency and dependability of VF-PMSM drives by enabling stable and accurate magnetization state control over a broad range of temperatures and speeds. Summing up, Lower magnet temperatures increase resistance to demagnetization, which raises the maximum torque at larger current phase angles, according to the results. On the other hand, higher temperatures change the magnetization trajectories, decrease torque capability, and facilitate demagnetization. Temperature has a significant impact on the controllability of the magnetization process, even though it was found to have little effect on the speed limit of d-axis pulse magnetization techniques at moderate magnetization levels. In order to prevent demagnetization, the closed-loop Straight-Line Stationary Frame Trajectory (CL-$SL\lambda^sT$) method dynamically modifies flux trajectories at each control period in response to real-time temperature input. Simulations and experiments showed that CL-$SL\lambda^sT$ successfully compensates for temperature-induced changes, guaranteeing stable magnetization control and successful changes in equivalent magnetization (J_{eq}) at 30 °C and 80 °C.

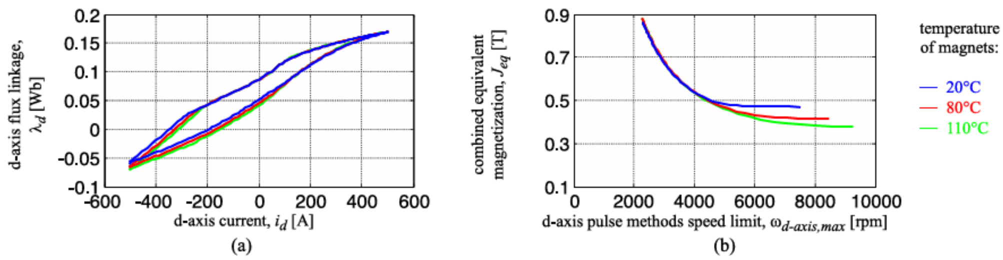

Figura 3.44: Effect of magnet temperature on magnetization and demagnetization of the test machine based on FEA: (a) d-axis flux linkage versus d-axis current; and (b) the estimated maximum speed where d-axis pulse methods can increase to a desired equivalent magnetization within the voltage limits of the inverter, neglecting the resistive voltage drop.
Source: [5]

Capitolo 4

Conclusions

This thesis has provided a comprehensive review and analysis of Variable Flux Memory Machines (VFMMs) and related variable-magnetization technologies, focusing on their operating principles, magnetic circuit architectures, control methods, and performance characteristics. From their earliest beginnings to the most sophisticated hybrid and variable-magnetization configurations suggested in recent literature, the study looked at the development of VFMM concepts. Instead of re-magnetizing the magnets themselves, the first researchers to work on VFMMs, who were first suggested by Ostović, proposed using adjustable magnetic circuits to control magnetic flux in permanent magnet machines. This flux-path control idea served as the basis for later VFMM studies, which purposefully use low-coercivity magnets to allow for active flux adjustment and reversible magnetization. The wide variety of VFMM topologies created over the last years has been the main focus of this thesis. The Series Hybrid VFMM is one of the earliest and most studied configurations and it has shown a good trade-off between torque density, magnetic stability and demagnetization resistance . In this topology the magnetic flux created by high coercivity permanent magnets passes through low coercivity magnets stabilizing their working point and improving the resistance to unintended demagnetization. However, the required magnetizing and demagnetizing currents are still relatively high and the achievable flux regulation range is typically limited compared to other designs.

The Parallel Hybrid VFMM is another configuration where magnetic paths of constant and variable permanent magnets are connected in parallel. This structure offers a higher capability of flux regulation and normally requires lower magnetizing currents; but the working point of the variable magnets is less stable and this configuration is more susceptible to unintentional demagnetization and magnetic cross-coupling effects.

To overcome the limitations of conventional hybrid configurations, a combined solution, the Hybrid Magnetic Circuit VFMM (HMC-VFMM), integrating both series and parallel magnetic paths, is proposed. This topology provides a better trade-off between flux regulation range and demagnetization resistance while achieving a relatively high efficiency over a wide operating area. The dual-layer magnetic circuit design provides more operational flexibility but it increases the complexity of the structure and manufacturing difficulties.

Another important class of VFMM technologies are switched flux based machines. The Hybrid-PM switched flux memory machine (SFMM) combines the concept of flux switching with the hybrid permanent magnet arrangements, allowing high torque density with efficient flux control. Similarly, the External-Rotor Switched Flux Memory Machine offers advantages in terms of torque capability and mechanical integration, particularly for applications that require a compact outer rotor design. The Fault-Tolerant Flux Switching Memory Machine has been designed to improve the reliability of applications that are safety critical. Its multi-phase configuration and distributed magnetic paths allow it to keep working even in the event of faults, making it especially suitable for electric vehicle traction systems and aerospace applications. However, this topology needs more complicated structural characteristics and increased control requirements.

Variable Magnetization Pattern Machines (VMPMs) offer a novel concept that the distribution of the magnetization in the permanent magnets can be dynamically manipulated. This allows flexible shaping of the torque-speed characteristics and extended operating ranges. A similar idea is implemented in the Variable-Magnetization Interior Permanent Magnet (VM-IPM) machine, where controllable magnetization states are added to the classical IPM rotor structures to allow for an increased field-weakening capability and a wider speed range operation. Different structural designs were investigated to offer a greater variety of structures for VFMM technologies. Axial-Field Juxtaposed Magnetic Circuit VFMM offers an axial magnetic path for high torque density and compact axial dimensions. The Dual-Sided VFMM further improves the magnetic utilization by the employment of two active air-gap regions, which augments the torque capability while maintaining a proper flux distribution.

Another analyzed design approach is the Variable Leakage Flux IPM Machine, where controlled magnetic leakage paths are used to control the air-gap flux levels. This allows us to control the performance of the machine dynamically without the need to continuously excite the field. However, care must be taken in designing the leakage barriers with the aim of not reducing efficiency. Material innovation has also helped in the recent development of VFMM. The use of advanced magnetic materials with high magnetic energy density and improved thermal stability is discussed in the Iron-Nitride-Based PM VFMM. These materials might minimize the dependence from rare-earth elements and optimize machine performance, but until now they have been confined to small-scale industrial applications.

Finally, the Hybrid-Excited Flux-Modulated Memory Machine is an advanced

configuration which includes permanent magnet excitation and auxiliary electromagnetic excitation. This approach provides a wide range of flux regulation and better controllability, and is therefore particularly appropriate for applications requiring variable speed operation and high efficiency in different operating areas.
In conclusion, the comparison of these topologies confirms the fact that no configuration of the VFMM can be considered as a universal optimum. Actually, each topology has its own set of benefits and limitations, depending on the requirements of the targeted application. Series configurations usually provide better magnetic stability and torque capability, whereas parallel and hybrid solutions allow for more flexibility in flux control. Switched-flux and hybrid excited machines expand the operational range, but they involve a greater complexity of design and control. Ultimately, a qualitative comparison of the topologies of the examined VFMMs is reported in Table 4.1. The considered machines are obtained from different studies and characterized by different dimensions, operating conditions and design targets, so the full quantitative comparison would not always be meaningful. Thus, the comparison is mainly based on relative trends concerning the torque capability and the effort needed for magnetization and demagnetization. Several important conclusions from this study can be summed up as follows:

- Three primary methods can be used to achieve flux controllability: remagnetization of low-coercivity PMs, magnetic leakage or bypass flux control, and hybrid circuits that combine the two effects.

- The choice of material is crucial: SmCo and NdFeB composites offer the best balance between coercivity, temperature stability, and magnetic energy density, while AlNiCo allows for reversible magnetization at a low energy cost.

- The best way to enhance the trade-off between torque density, efficiency, and flux-control range is still through topological innovation (series, parallel, hybrid, V-, Δ-, and U-shaped structures).

Finite-element and experimental results have verified the practical functionality, showing significant reductions in losses during flux-weakening operation and efficiency gains of up to 5%. Even with these developments, there are still research and engineering obstacles in VFMM technology. Predicting magnetization dynamics under transient current pulses requires precise hysteresis modelling of low-coercivity magnets. It is still unclear how to effectively control bidirectional magnetization without causing unwanted current stress or inverter oversizing. Additionally, advancements in sensor-less flux-state estimation, thermal management, and long-term magnet material stability are necessary for the integration of VFMMs into commercial electric powertrains. In summary, a promising alternative direction in the development of permanent magnet electrical drives is represented by variable flux memory machines. They provide a highly developed and effective way to

Tabella 4.1: Qualitative comparison of the analyzed VFMM topologies

Topology	**Torque Capability**	**Magnetization / Demagnetization Effort**
Series Hybrid VFMM	High	High
Parallel Hybrid VFMM	Medium	Low
Hybrid Magnetic Circuit VFMM (HMC-VFMM)	High	Medium
Hybrid-PM Switched Flux Memory Machine (SFMM)	High	Medium
External-Rotor Switched Flux Memory Machine	High	Medium
Fault-Tolerant Flux Switching Memory Machine	Medium	Medium–High
Variable Magnetization Pattern Machine (VMPM)	Medium	Low
Variable-Magnetization IPM (VM-IPM)	Medium–High	Medium
Axial-Field Juxtaposed Magnetic Circuit VFMM	High	Medium
Dual-Sided VFMM	High	Medium
Variable Leakage Flux IPM Machine	Medium–High	Low–Medium
Iron-Nitride-Based PM VFMM	High	Medium
Hybrid-Excited Flux-Modulated Memory Machine	High	Low

address the historical trade-off between efficient operation at high speed and high torque at low speed. The next generation of high-efficiency, wide-speed-range traction systems for electric and hybrid vehicles is anticipated to heavily rely on variable-magnetization IPM motors and VFMMs thanks to ongoing advancements in material science, magnetic circuit optimization and control techniques.

Bibliografia

[1] Ryoko Imamura e Robert D. Lorenz. «Stator Winding MMF Analysis for Variable Flux and Variable Magnetization Pattern PMSMs». In: *IEEE Transactions on Industry Applications* 56.3 (mag. 2020), pp. 2644–2653. ISSN: 0093-9994, 1939-9367. DOI: 10.1109/TIA.2020.2981605. URL: https://ieeexplore.ieee.org/document/9042235/ (visitato il 08/03/2024).

[2] Ryoko Imamura, Teng Wu e Robert D Lorenz. «Design of Variable Magnetization Pattern Machines for Dynamic Changes in the Back-EMF Waveform». In: ().

[3] Apoorva Athavale, David Reigosa, Kan Akatsu, Kazuto Sakai e Robert D. Lorenz. «Scalability and Key Tradeoffs of Variable Flux PM Machines for EV Traction Motor Systems». In: *2018 IEEE Energy Conversion Congress and Exposition (ECCE)*. Portland, OR, USA: IEEE, set. 2018, pp. 2292–2299. ISBN: 978-1-4799-7312-5. DOI: 10.1109/ECCE.2018.8558007. URL: https://ieeexplore.ieee.org/document/8558007/ (visitato il 08/03/2024).

[4] Apoorva Athavale, Kensuke Sasaki, Brent S. Gagas, Takashi Kato e Robert D. Lorenz. «Variable Flux Permanent Magnet Synchronous Machine (VF-PMSM) Design Methodologies to Meet Electric Vehicle Traction Requirements with Reduced Losses». In: *IEEE Transactions on Industry Applications* 53.5 (set. 2017), pp. 4318–4326. ISSN: 0093-9994, 1939-9367. DOI: 10.1109/TIA.2017.2701340. URL: http://ieeexplore.ieee.org/document/7919183/ (visitato il 08/03/2024).

[5] Brent S. Gagas, Kensuke Sasaki, Apoorva Athavale, Takashi Kato e Robert D. Lorenz. «Magnet Temperature Effects on the Useful Properties of Variable Flux PM Synchronous Machines and a Mitigating Method for Magnetization Changes». In: *IEEE Transactions on Industry Applications* 53.3 (mag. 2017), pp. 2189–2199. ISSN: 0093-9994, 1939-9367. DOI: 10.1109/TIA.2017.2674627. URL: http://ieeexplore.ieee.org/document/7864334/ (visitato il 08/03/2024).

[6] Hao Hua, Z. Q. Zhu, Adam Pride, Rajesh P. Deodhar e Toshinori Sasaki. «Comparison of End Effect in Series and Parallel Hybrid Permanent-Magnet Variable-Flux Memory Machines». In: *IEEE Transactions on Industry Applications* 55.3 (mag. 2019), pp. 2529–2537. ISSN: 0093-9994, 1939-9367. DOI: 10.1109/TIA.2018.2889979. URL: https://ieeexplore.ieee.org/document/8590752/ (visitato il 07/03/2024).

[7] Hao Hua, Z. Q. Zhu, Adam Pride, Rajesh P. Deodhar e Toshinori Sasaki. «A Novel Variable Flux Memory Machine With Series Hybrid Magnets». In: *IEEE Transactions on Industry Applications* 53.5 (set. 2017), pp. 4396–4405. ISSN: 0093-9994, 1939-9367. DOI: 10.1109/TIA.2017.2709261. URL: http://ieeexplore.ieee.org/document/7934364/ (visitato il 07/03/2024).

[8] Hao Hua, Z. Q. Zhu, Adam Pride, Rajesh Deodhar e Toshinori Sasaki. «Comparative Study on Variable Flux Memory Machines With Parallel or Series Hybrid Magnets». In: *IEEE Transactions on Industry Applications* 55.2 (mar. 2019), pp. 1408–1419. ISSN: 0093-9994, 1939-9367. DOI: 10.1109/TIA.2018.2879858. URL: https://ieeexplore.ieee.org/document/8526332/ (visitato il 07/03/2024).

[9] Takashi Kato, Robert Lorenz e Natee Limsuwan. «(54) VARABLE MAGNETIC FLUX-TYPE ROTARY ELECTRIC MACHINE».

[10] Kazuto Sakai, Kyouhei Yoneda e Wataru Suzuki. «Variable-Magnetization Interior Permanent Magnet Motor Yield Widely Variable Flux due to Small Magnetizing Current and Operating at High Power over a Wide Speed Range». In: *2021 IEEE Energy Conversion Congress and Exposition (ECCE)*. Vancouver, BC, Canada: IEEE, ott. 2021, pp. 4205–4212. ISBN: 978-1-7281-5135-9. DOI: 10.1109/ECCE47101.2021.9595578. URL: https://ieeexplore.ieee.org/document/9595578/ (visitato il 09/03/2024).

[11] Wataru Suzuki e Kazuto Sakai. «Variable-Magnetization IPM Motor for EVs with High Performance and Magnet Volume Reduction». In: *2022 International Conference on Electrical Machines (ICEM)*. Valencia, Spain: IEEE, set. 2022, pp. 361–366. ISBN: 978-1-6654-1432-6. DOI: 10.1109/ICEM51905.2022.9910750. URL: https://ieeexplore.ieee.org/document/9910750/ (visitato il 09/03/2024).

[12] Hai Xu, Jian Li, Junhua Chen, Yang Lu e Meng Ge. «Analysis of a Hybrid Permanent Magnet Variable-Flux Machine for Electric Vehicle Tractions Considering Magnetizing and Demagnetizing Current». In: *IEEE Transactions on Industry Applications* 57.6 (nov. 2021), pp. 5983–5992. ISSN: 0093-9994, 1939-9367. DOI: 10.1109/TIA.2021.3115077. URL: https://ieeexplore.ieee.org/document/9547714/ (visitato il 11/03/2024).

[13] Kyouhei Yoneda, Wataru Suzuki e Kazuto Sakai. «Designing a LEAF-Benchmark Variable Magnetization-IPM Motor with Two V-Shaped PMs at a 100 kW Power Level». In: *2022 IEEE Energy Conversion Congress and Exposition (ECCE)*. Detroit, MI, USA: IEEE, ott. 2022, pp. 1–7. ISBN: 978-1-7281-9387-8. DOI: 10.1109/ECCE50734.2022.9947861. URL: https://ieeexplore.ieee.org/document/9947861/ (visitato il 09/03/2024).

[14] Hui Yang, Wei Liu, Hao Zheng, Heyun Lin, Z. Q. Zhu, Fei Peng, Ya Li, Shukang Lyu e Xin Huang. «A Novel Delta-Type Hybrid-Magnetic-Circuit Variable Flux Memory Machine for Electrified Vehicle Applications». In: *IEEE Transactions on Transportation Electrification* 8.3 (set. 2022), pp. 3512–3523. ISSN: 2332-7782, 2372-2088. DOI: 10.1109/TTE.2022.3152894. URL: https://ieeexplore.ieee.org/document/9717249/ (visitato il 08/03/2024).

[15] Z. Q. Zhu, Hao Hua, Adam Pride, Rajesh Deodhar e Toshinori Sasaki. «Analysis and Reduction of Unipolar Leakage Flux in Series Hybrid Permanent-Magnet Variable Flux Memory Machines». In: *IEEE Transactions on Magnetics* 53.11 (nov. 2017), pp. 1–4. ISSN: 0018-9464, 1941-0069. DOI: 10.1109/TMAG.2017.2706764. URL: http://ieeexplore.ieee.org/document/7932474/ (visitato il 07/03/2024).

[16] Shukuan Zhang, Ping Zheng, Yong Liu, Mingqiao Wang, Guangyuan Qiao e Faliang Liu. «A High-Torque-Density Variable-Flux Memory Machine Utilizing Novel (Ce, Nd)-Fe-B Magnets». In: *IEEE Transactions on Magnetics* 57.2 (feb. 2021), pp. 1–6. ISSN: 0018-9464, 1941-0069. DOI: 10.1109/TMAG.2020.3006272. URL: https://ieeexplore.ieee.org/document/9130774/ (visitato il 08/03/2024).

[17] Qiang Wei, Zi Qiang Zhu, Seyedmilad Kazemisangdehi, Jianghua Feng, Shuying Guo, Yifeng Li e Shouzhi Feng. «A Novel Asymmetric U-Shaped Variable Flux Memory Machine». In: *2024 Third International Conference on Sustainable Mobility Applications, Renewables and Technology (SMART)*. Dubai, United Arab Emirates: IEEE, nov. 2024, pp. 1–8. ISBN: 979-8-3315-3292-5. DOI: 10.1109/SMART63170.2024.10815550. URL: https://ieeexplore.ieee.org/document/10815550/ (visitato il 11/11/2025).

[18] Qiang Wei, Zi Qiang Zhu, Seyedmilad Kazemisangdehi, Jianghua Feng, Shuying Guo, Yifeng Li e Shouzhi Feng. «A Novel Asymmetric Variable Flux Memory Machine with Hybrid-Layer Permanent Magnets». In: *2024 Third International Conference on Sustainable Mobility Applications, Renewables and Technology (SMART)*. Dubai, United Arab Emirates: IEEE, nov. 2024, pp. 1–9. ISBN: 979-8-3315-3292-5. DOI: 10.1109/SMART63170.2024.10815121. URL: https://ieeexplore.ieee.org/document/10815121/ (visitato il 11/11/2025).

[19] Hui Yang, Heyun Lin, Z. Q. Zhu, Shukang Lyu e Haitao Wang. «A Novel Dual-Layer PM Variable Flux Hybrid Memory Machine». In: *2018 IEEE Energy Conversion Congress and Exposition (ECCE)*. Portland, OR, USA: IEEE, set. 2018, pp. 262–268. ISBN: 978-1-4799-7312-5. DOI: 10.1109/ECCE.2018.8557973. URL: https://ieeexplore.ieee.org/document/8557973/ (visitato il 11/11/2025).

[20] Xifang Zhao, Heyun Lin, Wei Liu, Xianxian Zeng e Ya Li. «A New Series Variable Flux Memory Machine with Wide Flux Regulation Range». In: *2022 IEEE 20th Biennial Conference on Electromagnetic Field Computation (CEFC)*. Denver, CO, USA: IEEE, ott. 2022, pp. 1–2. ISBN: 978-1-6654-6833-6. DOI: 10.1109/CEFC55061.2022.9940719. URL: https://ieeexplore.ieee.org/document/9940719/ (visitato il 11/11/2025).

[21] Qiang Wei, Zi Qiang Zhu, Jianghua Feng, Shuying Guo, Yifeng Li e Shouzhi Feng. «A Novel Asymmetric Split-Spoke-Type Variable Flux Memory Machine». In: *2024 Third International Conference on Sustainable Mobility Applications, Renewables and Technology (SMART)*. Dubai, United Arab Emirates: IEEE, nov. 2024, pp. 1–8. ISBN: 979-8-3315-3292-5. DOI: 10.1109/SMART63170.2024.10815120. URL: https://ieeexplore.ieee.org/document/10815120/ (visitato il 11/11/2025).

[22] Hui Yang, Heyun Lin, Z. Q. Zhu, Shukang Lyu e Keyi Wang. «A Novel Dual-Sided PM Variable Flux Memory Machine». In: *IEEE Transactions on Magnetics* 54.11 (nov. 2018), pp. 1–5. ISSN: 0018-9464, 1941-0069. DOI: 10.1109/TMAG.2018.2845870. URL: https://ieeexplore.ieee.org/document/8405362/ (visitato il 11/11/2025).

[23] Yuming Yan, Fawen Shen, Shanmukha Ramakrishna, Gajanayake Chandana Jayampathi, Shuai Wang e Christopher H.T. Lee. «A Novel Fault Tolerant Flux Switching Memory Machine with Highly Flux-Controllability». In: *IECON 2021 – 47th Annual Conference of the IEEE Industrial Electronics Society*. Toronto, ON, Canada: IEEE, ott. 2021, pp. 1–6. ISBN: 978-1-6654-3554-3. DOI: 10.1109/IECON48115.2021.9589836. URL: https://ieeexplore.ieee.org/document/9589836/ (visitato il 11/11/2025).

[24] Xianxian Zeng, Heyun Lin, Yuxiang Zhong, Xifang Zhao, Hui Yang e Xiping Liu. «A Novel Hybrid Magnetic Circuit Dual-Variable Flux Memory Machine for EV Traction». In: *IEEE Transactions on Transportation Electrification* 11.2 (apr. 2025), pp. 5337–5347. ISSN: 2332-7782, 2372-2088. DOI: 10.1109/TTE.2024.3478335. URL: https://ieeexplore.ieee.org/document/10714481/ (visitato il 11/11/2025).

[25] Y. Mao e S. X. Niu. «A novel hybrid-excited flux-modulated memory machine for electrical continuously variable transmission system». In: *2017 7th International Conference on Power Electronics Systems and Applications - Smart Mobility, Power Transfer & Security (PESA)*. Hong Kong: IEEE, dic. 2017, pp. 1–5. ISBN: 978-1-5386-1387-0. DOI: 10.1109/PESA.2017.8277741. URL: http://ieeexplore.ieee.org/document/8277741/ (visitato il 11/11/2025).

[26] Hui Yang, Shukang Lyu, Heyun Lin, Zi-qiang Zhu, Hao Zheng e Tiangang Wang. «A Novel Hybrid-Magnetic-Circuit Variable Flux Memory Machine». In: *IEEE Transactions on Industrial Electronics* 67.7 (lug. 2020), pp. 5258–5268. ISSN: 0278-0046, 1557-9948. DOI: 10.1109/TIE.2019.2931494. URL: https://ieeexplore.ieee.org/document/8786909/ (visitato il 11/11/2025).

[27] Xianxian Zeng, Heyun Lin, Xifang Zhao, Yuxiang Zhong e Hui Yang. «A Novel Parallel Magnetic Circuit Variable Flux Machine by Employing Flux Leakage». In: *2023 IEEE 6th Student Conference on Electric Machines and Systems (SCEMS)*. HuZhou, China: IEEE, dic. 2023, pp. 1–5. ISBN: 979-8-3503-2934-6. DOI: 10.1109/SCEMS60579.2023.10379253. URL: https://ieeexplore.ieee.org/document/10379253/ (visitato il 11/11/2025).

[28] Hui Yang, Heyun Lin, Z. Q. Zhu, Dong Wang, Shuhua Fang e Yunkai Huang. «A Variable-Flux Hybrid-PM Switched-Flux Memory Machine for EV/HEV Applications». In: *IEEE Transactions on Industry Applications* 52.3 (mag. 2016), pp. 2203–2214. ISSN: 0093-9994, 1939-9367. DOI: 10.1109/TIA.2016.2524400. URL: http://ieeexplore.ieee.org/document/7398043/ (visitato il 11/11/2025).

[29] Hui Yang, Hao Zheng, Shukang Lyu, Heyun Lin, Zi-Qiang Zhu e Weinong Fu. «Analysis of Flux Regulation Principle in a Novel Hybrid-Magnet-Circuit Variable Flux Memory Machine». In: *2019 22nd International Conference on Electrical Machines and Systems (ICEMS)*. Harbin, China: IEEE, ago. 2019, pp. 1–6. ISBN: 978-1-7281-3398-0. DOI: 10.1109/ICEMS.2019.8921563. URL: https://ieeexplore.ieee.org/document/8921563/ (visitato il 11/11/2025).

[30] Hui Yang, Hao Zheng, Heyun Lin, Z. Q. Zhu, Jiaxing Lei, Wei Liu e Shukang Lyu. «Analysis of Novel Hybrid-Magnet-Circuit Variable Flux Memory Machines with Different Magnet Arrangements». In: *2019 IEEE Energy Conversion Congress and Exposition (ECCE)*. Baltimore, MD, USA: IEEE, set. 2019, pp. 251–258. ISBN: 978-1-7281-0395-2. DOI: 10.1109/ECCE.2019.8913296. URL: https://ieeexplore.ieee.org/document/8913296/ (visitato il 11/11/2025).

[31] Guangyuan Qiao, Ping Zheng, Mingqiao Wang, Faliang Liu e Yong Liu. «Design, modelling and analysis of a hybrid-magnet variable-flux PMSM with variable series-parallel magnetic circuit». In: *Energy Reports* 8 (ago. 2022), pp. 1200–1209. ISSN: 23524847. DOI: 10.1016/j.egyr.2022.02.233. URL: https://linkinghub.elsevier.com/retrieve/pii/S2352484722004784 (visitato il 11/11/2025).

[32] Zhigang Hu, Xiping Liu, Zhangqi Liu, Zhiguo Huang, Wenliang Hu e Zihao Shi. «Design and Analysis of Wide Speed-Regulated Reverse Salient-Pole Variable Leakage Flux Interior Permanent Magnet Machine». In: *2023 IEEE 6th Student Conference on Electric Machines and Systems (SCEMS)*. HuZhou, China: IEEE, dic. 2023, pp. 1–6. ISBN: 979-8-3503-2934-6. DOI: 10.1109/SCEMS60579.2023.10379209. URL: https://ieeexplore.ieee.org/document/10379209/ (visitato il 11/11/2025).

[33] Xianxian Zeng, Heyun Lin, Ya Li e Xifang Zhao. «Design and Investigation of a New Variable Flux Memory Machine with Self-Flux Leakage Path». In: *2022 IEEE 20th Biennial Conference on Electromagnetic Field Computation (CEFC)*. Denver, CO, USA: IEEE, ott. 2022, pp. 1–2. ISBN: 978-1-6654-6833-6. DOI: 10.1109/CEFC55061.2022.9940885. URL: https://ieeexplore.ieee.org/document/9940885/ (visitato il 11/11/2025).

[34] Xianxian Zeng, Heyun Lin, Yuxiang Zhong, Xifang Zhao, Hui Yang e Xiping Liu. «Design Concept and Performance Analysis of Dual-Variable Flux Memory Machines for Traction Drive». In: *IEEE Transactions on Transportation Electrification* 11.1 (feb. 2025), pp. 2171–2180. ISSN: 2332-7782, 2372-2088. DOI: 10.1109/TTE.2024.3417693. URL: https://ieeexplore.ieee.org/document/10568185/ (visitato il 11/11/2025).

[35] Bassam S. Abdel-Mageed, Akrem M. Aljehaimi, Benoit Blanchard St-Jacques, Ruisheng Shi e Pragasen Pillay. «Design of Iron-Nitride-Based Permanent Magnet Variable Flux Motors». In: *IECON 2024 - 50th Annual Conference of the IEEE Industrial Electronics Society*. Chicago, IL, USA: IEEE, nov. 2024, pp. 1–6. ISBN: 978-1-6654-6454-3. DOI: 10.1109/IECON55916.2024.10905478. URL: https://ieeexplore.ieee.org/document/10905478/ (visitato il 11/11/2025).

[36] Wei Liu, Hui Yang, Heyun Lin, Hanlin Zhan, Wenjie Chen, Di Wu e Minghu Yu. «Design Tradeoff Between Saliency Ratio and PM Flux Linkage in Variable Flux Memory Machines». In: *IEEE Transactions on Energy Conversion* 38.1 (mar. 2023), pp. 562–572. ISSN: 0885-8969, 1558-0059. DOI: 10.1109/TEC.2022.3199768. URL: https://ieeexplore.ieee.org/document/9861680/ (visitato il 11/11/2025).

[37] Qiang Wei, Z.Q. Zhu, Yan Jia, Jianghua Feng, Shuying Guo, Yifeng Li e Shouzhi Feng. «Electromagnetic Performance Analysis of Variable Flux Memory Machines with Series-magnetic-circuit and Different Rotor Topologies». In: *CES Transactions on Electrical Machines and Systems* 8.1 (mar. 2024), pp. 3–11. ISSN: 2096-3564. DOI: 10.30941/CESTEMS.2024.00012. URL: https://ieeexplore.ieee.org/document/10488427/ (visitato il 11/11/2025).

[38] Xifang Zhao, Heyun Lin, Yuxiang Zhong, Hui Yang, Xianxian Zeng e Xiping Liu. «Evolution and Analysis of Leakage Flux Path for Memory Machine With Variable Leakage Flux Capability». In: *IEEE Transactions on Transportation Electrification* 11.5 (ott. 2025), pp. 12453–12462. ISSN: 2332-7782, 2372-2088. DOI: 10.1109/TTE.2025.3590751. URL: https://ieeexplore.ieee.org/document/11087395/ (visitato il 11/11/2025).

[39] Hui Yang, Heyun Lin, Z. Q. Zhu, Kaikai Guo, Dong Wang, Shuhua Fang e Yunkai Huang. «Flux-Concentrated External-Rotor Switched Flux Memory Machines for Direct-Drive Applications». In: *IEEE Transactions on Applied Superconductivity* 26.7 (ott. 2016), pp. 1–6. ISSN: 1051-8223, 1558-2515. DOI: 10.1109/TASC.2016.2600589. URL: http://ieeexplore.ieee.org/document/7544473/ (visitato il 11/11/2025).

[40] Guangyuan Qiao, Ping Zheng, Mingqiao Wang, Faliang Liu e Yong Liu. «Design, modelling and analysis of a hybrid-magnet variable-flux PMSM with variable series-parallel magnetic circuit». In: *Energy Reports* 8 (ago. 2022), pp. 1200–1209. ISSN: 23524847. DOI: 10.1016/j.egyr.2022.02.233. URL: https://linkinghub.elsevier.com/retrieve/pii/S2352484722004784 (visitato il 11/11/2025).

[41] Xianxian Zeng, Heyun Lin, Hui Yang, Yuxiang Zhong, Xifang Zhao e Xiping Liu. «Impacting Mechanism of Variable Leakage Flux on Magnetizing and Demagnetizing Effects in Dual-Variable Flux Memory Machines for EV Traction». In: *IEEE Transactions on Transportation Electrification* 11.3 (giu. 2025), pp. 8202–8212. ISSN: 2332-7782, 2372-2088. DOI: 10.1109/TTE.2025.3538321. URL: https://ieeexplore.ieee.org/document/10887047/ (visitato il 11/11/2025).

[42] Wei Liu, Hui Yang, Heyun Lin e Xiping Liu. «Influence of Low-Coercive-Force Magnet Property on Electromagnetic Performance of Variable Flux Memory Machine». In: *IEEE Transactions on Magnetics* 58.8 (ago. 2022), pp. 1–6. ISSN: 0018-9464, 1941-0069. DOI: 10.1109/TMAG.2022.3153285. URL: https://ieeexplore.ieee.org/document/9718296/ (visitato il 11/11/2025).

[43] Hui Yang, Yongsheng Ge e Heyun Lin. «Influence of Rotor Pole Number on Electromagnetic Performance of Hybrid-Magnetic-Circuit Variable Flux Memory Machine». In: *2021 IEEE Sustainable Power and Energy Conference (iSPEC)*. Nanjing, China: IEEE, dic. 2021, pp. 3478–3482. ISBN: 978-1-6654-1439-5. DOI: 10.1109/iSPEC53008.2021.9735646. URL: https://ieeexplore.ieee.org/document/9735646/ (visitato il 11/11/2025).

[44] Hao Hua, Zicheng Zhou e Wei Hua. «Investigation of Dual-Effect Air-Gap Field Regulation Mechanism in Variable Flux Memory Machines». In: *IEEE Transactions on Industrial Electronics* 71.8 (ago. 2024), pp. 8571–8580. ISSN: 0278-0046, 1557-9948. DOI: 10.1109/TIE.2023.3312444. URL: https://ieeexplore.ieee.org/document/10269449/ (visitato il 11/11/2025).

[45] Hui Yang, Ling Qin, Heyun Lin e Z. Q. Zhu. «Investigation of Torque Characteristics of Switched Flux Hybrid Magnet Memory Machine by a Coupled Solution». In: *IEEE Transactions on Magnetics* 56.4 (apr. 2020), pp. 1–5. ISSN: 0018-9464, 1941-0069. DOI: 10.1109/TMAG.2019.2953825. URL: https://ieeexplore.ieee.org/document/8957352/ (visitato il 11/11/2025).

[46] Zicheng Zhou, Hao Hua e Bohu Zhang. «Investigation of Variable Flux Memory Machines with Hybrid Connected Delta-Type Permanent Magnets». In: *2021 IEEE 4th Student Conference on Electric Machines and Systems (SCEMS)*. Huzhou, China: IEEE, dic. 2021, pp. 01–07. ISBN: 978-1-6654-3681-6. DOI: 10.1109/SCEMS52239.2021.9646149. URL: https://ieeexplore.ieee.org/document/9646149/ (visitato il 11/11/2025).

[47] Rui Tu, Hui Yang, Heyun Lin, Hanlin Zhan e Chaohui Liu. «Magnet Pole Design Improvement of Novel Hybrid-Pole Variable Flux Memory Machine». In: *2023 IEEE Energy Conversion Congress and Exposition (ECCE)*. Nashville, TN, USA: IEEE, ott. 2023, pp. 4338–4345. ISBN: 979-8-3503-1644-5. DOI: 10.1109/ECCE53617.2023.10362848. URL: https://ieeexplore.ieee.org/document/10362848/ (visitato il 11/11/2025).

[48] Yuan Gao, Yaojing Feng, Chenxi Xia, Bo Long e Shoudao Huang. «Novel Axial-Field Juxtaposed Magnetic Circuit Variable Flux Memory Machine». In: *2024 IEEE International Magnetic Conference (INTERMAG)*. Rio de Janeiro, Brazil: IEEE, mag. 2024, pp. 1–5. ISBN: 979-8-3503-7171-0. DOI: 10.1109/INTERMAG56625.2024.10830463. URL: https://ieeexplore.ieee.org/document/10830463/ (visitato il 11/11/2025).